Table 1. Age- and sex-specific prevalence of dementia

	Population at risk	All types		AD		VD		DLB		PDD		PSP		FTLD		Others	
		cases	prevalence	cases	prevalence	cases	prevalence	cases	prevalence	cases	prevalence	cases	prevalence	cases	prevalence	cases	prevalence
Both sexes																	
65–69 years	178	2	1.1	–	–	1	0.56	–	–	1	0.56	–	–	–	–	–	–
70–74 years	206	10	4.9	4	1.9	4	1.9	–	–	–	–	–	–	1	0.49	1	0.49
75–79 years	226	19	8.4	10	4.4	4	1.8	1	0.44	1	0.44	–	–	–	–	3	1.3
80–84 years	161	22	13.7	16	9.9	2	1.2	1	0.62	–	–	2	1.2	–	–	1	0.62
85–89 years	114	27	23.7	18	15.8	1	0.88	3	2.6	4	3.5	–	–	–	–	1	0.88
90– years	58	24	41.4	18	31.0	4	6.9	–	–	1	1.72	–	–	–	–	1	1.7
Total	943	104	11.0	66	7.0	16	1.7	5	0.53	7	0.74	2	0.21	1	0.11	7	0.74
Men																	
65–69 years	87	1	1.2	–	–	–	–	–	–	1	1.2	–	–	–	–	–	–
70–74 years	90	6	6.7	2	2.2	2	2.2	–	–	–	–	–	–	1	1.1	1	1.1
75–79 years	99	8	8.1	2	2.0	2	2.0	1	1.0	–	–	–	–	–	–	3	3.0
80–84 years	52	6	11.5	2	3.8	2	3.8	–	–	–	–	2	3.9	–	–	–	–
85–89 years	43	7	16.3	2	4.7	1	2.3	2	4.7	1	2.3	–	–	–	–	1	2.3
90– years	15	5	33.3	4	26.7	–	–	–	–	–	–	–	–	–	–	1	6.7
Total	386	33	8.5	12	3.1	7	1.8	3	0.78	2	0.52	2	0.52	1	0.26	6	1.6
Women																	
65–69 years	91	1	1.1	–	–	1	1.1	–	–	–	–	–	–	–	–	–	–
70–74 years	116	4	3.4	2	1.7	2	1.7	–	–	–	–	–	–	–	–	–	–
75–79 years	127	11	8.7	8	6.3	2	1.6	–	–	1	0.79	–	–	–	–	–	–
80–84 years	109	16	14.7	14	12.8	–	–	1	0.92	–	–	–	–	–	–	1	0.92
85–89 years	71	20	28.2	16	22.5	–	–	1	1.4	3	4.2	–	–	–	–	–	–
90– years	43	19	44.2	14	32.6	4	9.3	–	–	1	2.3	–	–	–	–	–	–
Total	557	71	12.7	54	9.7	9	1.6	2	0.36	5	0.90	–	–	–	–	1	0.18

Prevalence = cases/100.

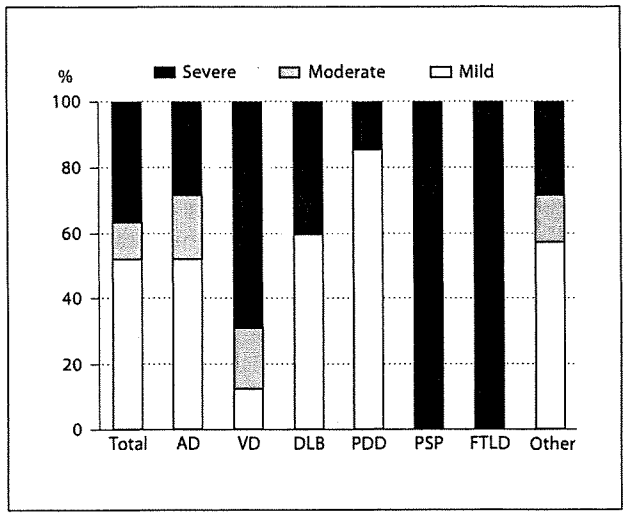

Fig. 3. Severity of subtypes of dementia.

in men. The prevalence was 0.53 (95% CI 0.07–0.99) for DLB and 0.74 (95% CI 0.19–1.3) for PDD. The AD/DLB ratio in both sexes was 13.2. The severity of dementia according to FAST is shown in figure 3. Fifty-four (52.0%) were at the mild stage, 12 (11.5%) at the moderate stage, and 38 (36.5%) were at the severe stage. In AD, most subjects were at the mild stage; however, in VD, most subjects were at the severe stage. Fifty-four (52%) were living in their home and 50 (48%) were living in a nursing home in town.

Discussion

We investigated the prevalence of dementia in an isolated rural island community in western Japan. We selected this town for the following reasons: (1) the public health nurses working as the sole permanent care providers have been keeping detailed information about the physical and mental health of the entire town for over 20

years; (2) active collaboration was offered by family doctors in the town; (3) this town is a rural island with a stable population, and only a few demented subjects move to nursing homes in other areas.

Our study showed that the prevalence of all types of dementia in the elderly population aged 65 years and older was 11.0 in a rural community in Japan. This finding is higher than that of previous Japanese reports showing a prevalence of 3.8–8.5 [3–5, 17–19]. There are some possible reasons for the higher prevalence of dementia found in our study. The first is the relatively higher proportion of subjects in the population aged 65 years and older in the town studied. Second, we surveyed all the demented subjects including those instituted in the nursing home in town, where severely demented subjects are living. Thus, our study indicated a relatively higher prevalence of subjects with severe dementia. Third, we achieved a very high response rate in this survey, due to the outstanding contribution of the public health nurses.

In agreement with recent epidemiological studies in Japan, our study showed that AD is the most common and VD is the second most common subtype of dementia amongst all types of dementia in elderly people [3–5,17, 19]. We also examined the prevalence of subtypes of dementia other than AD and VD. The prevalence was 0.53 for DLB in our study. Some epidemiologic data on DLB are available from a community-based survey. The prevalence of DLB in the general population is reported to be from 0 to 5 [20]. Yamada et al. [17] reported that the prevalence of DLB in Japan among subjects aged 65 years and older was 0.1. Yokota et al. [21] reported the AD/DLB ratio to be 12.9 in their study based on a hospital memory clinic in Japan. The AD/DLB ratio in our study was 13.2, which was consistent with their study. We also examined the prevalence of PDD in the same community. Although several studies found a prevalence of DLB or PDD, few have reported a simultaneous prevalence in a community. DLB and PDD share many pathological and clinical features [22]. The time course of the symptoms and presenting features primarily differentiate these disorders. In this study, the 1-year rule between the onset of dementia and parkinsonism was adapted to distinguish between DLB and PDD. The PDD patients were reliably diagnosed amongst PD patients who had been diagnosed by the UK PD Brain Bank clinical diagnostic criteria [23]. In our study, the prevalence of PDD was 0.74, which was higher than that of DLB. After a systematic review, Arsland et al. [24] reported a 0.2–0.5 prevalence of PDD in the general population. Our results appear to be consistent with this finding.

Only 1 subject was diagnosed as having FTLD in our study. A high frequency of FTLD patients has been reported amongst subjects aged <65 years, but not in subjects aged 65 years and older in Western countries [25, 26]. After their hospital-based study in Japan, Yokota et al. [21] reported that FTLD was the second most common neurodegenerative dementia following AD amongst those with early-onset dementia, but it was very rare amongst late-onset patients. Among 3,715 subjects >65 years of age, Yamada et al. [17] found that none were diagnosed with FTLD, and Ikeda et al. [18] reported only 2 subjects with FTLD among 1,438 subjects aged >64 years in their community-based study in Japan. Our data are consistent with these community-based studies. There is a lack of valid and reliable methods for screening the core clinical features by which FTLD is usually identified, so FTLD can be difficult to diagnose in the community.

This study is a door-to-door, 2-phase design based on phase 1 screening by highly educated public health nurses and on phase 2 diagnosis by a neurologist. Some limitations of this study have to be considered. One important limitation was the relatively small size of the population surveyed, and our estimations of subtypes of dementia are based on a small number of cases. Second, we mainly evaluated brain imaging of the subjects by CT scan; however, magnetic resonance imaging detects abnormal findings more sensitively than CT. Third, although all diagnoses in this study were made according to the most recent clinical diagnostic criteria, no patients were neuropathologically diagnosed with subtypes of dementia.

In conclusion, we showed the prevalence of dementia in the elderly population aged 65 years and older in a rural area in Japan to be 11.0 cases/100 population, which is higher than that found by previous epidemiological studies in Japan.

Acknowledgments

We thank all the inhabitants of Ama-cho for their participation in the present study. We also thank Dr. Sakakibara, Dr. Kitagawa, Ms. Hamami, Ms. Nakagawa, Ms. Ikeda and Ms. Yoshino for collecting and providing clinical information. This study was supported, in part, by a Grant-in-Aid for Scientific Research from the Ministry of Education, Culture, Sports, Science and Technology, Government of Japan (to K.N.).

References

1 Ueda K, Kawano H, Hasuo Y, Fujishima M: Prevalence and etiology of dementia in a Japanese community. Stroke 1992;23:798–803.
2 Hatada K, Okazaki Y, Yoshitake K, Takada K, Nakane Y: Further evidence of westernization of dementia prevalence in Nagasaki, Japan, and family recognition. Int Psychogeriatr 1999;11:123–138.
3 Urakami K, Adachi Y, Wakutani Y, Isoe K, Ji Y, Takahashi K, Nakashima K: Epidemiologic and genetic studies of dementia of the Alzheimer type in Japan. Dement Geriatr Cogn Disord 1998;9:294–298.
4 Shiba M, Shimogaito J, Kose A, Fujiuchi S, Nishiyama H, Yoshimasu F, Asai T, Rocca WA: Prevalence of dementia in the rural village of Hanazono-mura, Japan. Neuroepidemiology 1999;18:32–36.
5 Wakutani Y, Kusumi M, Wada K, Kawasima M, Ishizaki K, Mori M, Mori N, Ijiri T, Adachi Y, Ashida Y Kuno N, Urakami K, Takeshima T, Nakashima K: Longitudinal changes in the prevalence of dementia in a Japanese rural area. Psychogeriatrics 2007;7:150–154.
6 Folstein MF, Folstein SE, McHugh PR: 'Mini-mental state'. A practical method for grading the cognitive state of patients for the clinician. J Psychiatr Res 1975;12:189–198.
7 Blessed G, Tomlinson BE, Roth M: The association between quantitative measures of dementia and of senile change in the cerebral gray matter of elderly subjects. Br J Psychiatry 1968;114:797–811.
8 Granger CV, Rewis LS, Peters NC, Sherwood CC, Barrett JE: Stroke rehabilitation – analysis of repeated Barthel index measures. Arch Phys Med Rehabil 1979;60:14–17.
9 American Psychiatric Association: Diagnostic and Statistical Manual of Mental Disorders, ed 4. Washington, American Psychiatric Association, 1994.
10 McKhann G, Drachman D, Folstein M, Katzman R, Price D, Stadlan EM: Clinical diagnosis of Alzheimer's disease: report of the NINCDS-ADRDA Work Group under the auspices of Department of Health and Human Services Task Force on Alzheimer's Disease. Neurology 1984;34:939–944.
11 Roman GC, Tatemichi TK, Erkinjuntti T, Cummings JL, Masdeu JC, Garcia JH, Amaducci L, Brun A, Hofman A, Moody DM, O'Brien MD, Yamaguchi T, Grafman J, Drayer BP, Bennett DA, Fisher M, Ogata J, Kokmen E, Bermejo F, Wolf PA, Gorelick PB, Bick KL, Pajeau AK, Bell MA, DeCarli C, Culebras A, Korczyn AD, Bogousslavsky J, Hartmann A, Scheinberg P: Vascular dementia: diagnostic criteria for research studies: report of the NINDS-AIREN International Workshop. Neurology 1993;43:250–260.
12 McKeith IG, Dickson DW, Lowe J, Emre M, O'Brien JT, Feldman H, Cummings J, Duda JE, Lippa C, Perry EK, Aarsland D, Arai H, Ballard CG, Boeve B, Burn DJ, Costa D, Del Ser T, Dubois B, Galasko D, Gauthier S, Goetz CG, Gomez-Tortosa E, Halliday G, Hansen LA, Hardy J, Iwatsubo T, Kalaria RN, Kaufer D, Kenny RA, Korczyn A, Kosaka K, Lee VM, Lees A, Litvan I, Londos E, Lopez OL, Minoshima S, Mizuno Y, Molina JA, Mukaetova-Ladinska EB, Pasquier F, Perry RH, Schulz JB, Trojanowski JQ, Yamada M, Consortium on DLB: Diagnosis and management of dementia with Lewy bodies: third report of the DLB Consortium. Neurology 2005;65:1863–1872.
13 Emre M, Aarsland D, Brown R, Burn DJ, Duyckaerts C, Mizuno Y, Broe GA, Cummings J, Dickson DW, Gauthier S, Goldman J, Goetz C, Korczyn A, Lees A, Levy R, Litvan I, McKeith I, Olanow W, Poewe W, Quinn N, Sampaio C, Tolosa E, Dubois B: Clinical diagnostic criteria for dementia associated with Parkinson's disease. Mov Disord 2007;22:1689–1707.
14 Litvan I, Agid Y, Calne D, Campbell G, Dubois B, Duvoisin RC, Goetz CG, Golbe LI, Grafman J, Growdon JH, Hallett M, Jankovic J, Quinn NP, Tolosa E, Zee DS: Clinical research criteria for the diagnosis of progressive supranuclear palsy (Steele-Richardson-Olszewski syndrome): report of the NINDS-SPSP international workshop. Neurology 1996;47:1–9.
15 Neary D, Snowden JS, Gustafson L, Passant U, Stuss D, Black S, Freedman M, Kertesz A, Robert PH, Albert M, Boone K, Miller BL, Cummings J, Benson DF: Frontotemporal lobar degeneration: a consensus on clinical diagnostic criteria. Neurology 1998;51:1546–1554.
16 Reisberg B: Dementia: a systematic approach to identifying reversible causes. Geriatrics 1986;41:30–46.
17 Yamada T, Hattori H, Miura A, Tanabe M, Yamori Y: Prevalence of Alzheimer's disease, vascular dementia and dementia with Lewy bodies in a Japanese population. Psychiatry Clin Neurosci 2001;55:21–25.
18 Ikeda M, Hokoishi K, Maki N, Nebu A, Tachibana N, Komori K, Shigenobu K, Fukuhara R, Tanabe H: Increased prevalence of vascular dementia in Japan: a community-based epidemiological study. Neurology 2001;57:839–844.
19 Meguro K, Ishii H, Yamaguchi S, Ishizaki J, Shimada M, Sato M, Hashimoto R, Shimada Y, Meguro M, Yamadori A, Sekita Y: Prevalence of dementia and dementing diseases in Japan: the Tajiri project. Arch Neurol 2002;59:1109–1114.
20 Zaccai J, McCracken C, Brayne C: A systematic review of prevalence and incidence studies of dementia with Lewy bodies. Age Ageing 2005;34:561–566.
21 Yokota O, Sasaki K, Fujisawa Y, Takahashi J, Terada S, Ishihara T, Nakashima H, Kugo A, Ata T, Ishizu H, Kuroda S: Frequency of early and late-onset dementias in a Japanese memory disorders clinic. Eur J Neurol 2005;12:782–790.
22 McKeith IG, Burn D: Spectrum of Parkinson's disease, Parkinson's dementia, and Lewy body dementia; in DeKosky ST (ed): Neurologic Clinics. Philadelphia, Saunders, 2000, pp 865–883.
23 Hughes AJ, Daniel SE, Blankson S, Lees AJ: A clinicopathologic study of 100 cases of Parkinson's disease. Arch Neurol 1993;50:140–148.
24 Aarsland D, Zaccai J, Brayne C: A systematic review of prevalence studies of dementia in Parkinson's disease. Mov Disord 2005;20:1255–1263.
25 Vraamark Elberling T, Stokholm J, Høgh P, Waldemar G: Diagnostic profile of young and middle-aged memory clinic patients. Neurology 2002;59:1259–1262.
26 Ratnavalli E, Brayne C, Dawson K, Hodges JR: The prevalence of frontotemporal dementia. Neurology 2002;58:1615–1621.

OPEN ACCESS Freely available online

PLoS one

A Novel Form of Memory for Auditory Fear Conditioning at a Low-Intensity Unconditioned Stimulus

Ayumi Kishioka[1], Fumiaki Fukushima[1], Tamae Ito[1], Hirotaka Kataoka[1], Hisashi Mori[1¤a], Toshio Ikeda[2¤b], Shigeyoshi Itohara[2], Kenji Sakimura[3], Masayoshi Mishina[1]*

1 Department of Molecular Neurobiology and Pharmacology, Graduate School of Medicine, University of Tokyo, Tokyo, Japan, 2 Laboratory of Behavioral Genetics, Brain Science Institute, RIKEN, Saitama, Japan, 3 Department of Cellular Neurobiology, Brain Research Institute, Niigata University, Niigata, Japan

Abstract

Fear is one of the most potent emotional experiences and is an adaptive component of response to potentially threatening stimuli. On the other hand, too much or inappropriate fear accounts for many common psychiatric problems. Cumulative evidence suggests that the amygdala plays a central role in the acquisition, storage and expression of fear memory. Here, we developed an inducible striatal neuron ablation system in transgenic mice. The ablation of striatal neurons in the adult brain hardly affected the auditory fear learning under the standard condition in agreement with previous studies. When conditioned with a low-intensity unconditioned stimulus, however, the formation of long-term fear memory but not short-tem memory was impaired in striatal neuron-ablated mice. Consistently, the ablation of striatal neurons 24 h after conditioning with the low-intensity unconditioned stimulus, when the long-term fear memory was formed, diminished the retention of the long-term memory. Our results reveal a novel form of the auditory fear memory depending on striatal neurons at the low-intensity unconditioned stimulus.

Citation: Kishioka A, Fukushima F, Ito T, Kataoka H, Mori H, et al. (2009) A Novel Form of Memory for Auditory Fear Conditioning at a Low-Intensity Unconditioned Stimulus. PLoS ONE 4(1): e4157. doi:10.1371/journal.pone.0004157

Editor: David S. Vicario, Rutgers University, United States of America

Received September 9, 2008; **Accepted** November 23, 2008; **Published** January 9, 2009

Funding: This work was supported in part by Grant-in-Aid for Scientific Research on Priority Areas (Molecular Brain Science) and Global COE Program (Integrative Life Science Based on the Study of Biosignaling Mechanisms) from the Ministry of Education, Culture, Sports, Science and Technology of Japan. F.F. was supported by Japan Society for the Promotion of Science. The funders had no role in study design, data collection and analysis, decision to publish, or preparation of the manuscript.

Competing Interests: The authors have declared that no competing interests exist.

* E-mail: mishina@m.u-tokyo.ac.jp

¤a Current address: Department of Molecular Neuroscience, Graduate School of Medicine and Pharmaceutical Sciences, University of Toyama, Toyama, Japan
¤b Current address: Laboratory of Experimental Animal Model Research, National Center for Geriatrics and Gerontology, Obu, Japan

Introduction

Fear is one of the most potent emotional experiences of our lifetime and is an adaptive component of response to potentially threatening stimuli, serving a function that is critical to the survival of higher vertebrates [1,2]. Too much or inappropriate fear, however, accounts for many common psychiatric problems [3–5]. A fearful experience can establish an emotional memory that results in permanent behavioral changes and emotional memories have been observed in many animal groups [6]. The brain mechanisms underlying fear are similar in different species and the fear system will respond similarly in a person or a rodent, using a limited set of defense response strategies [7]. The memory of learned fear can be assessed quantitatively using a Pavlovian fear-conditioning paradigm [1,2]. During fear conditioning, an initially neutral conditioned stimulus (CS, e.g. an auditory tone) acquires biological significance by becoming associated with an aversive unconditioned stimulus (US, e.g. a footshock). After learning this association, an animal responds to the previously neutral CS with a set of defensive behavioral responses, such as freezing. Anatomical tracing and lesion studies demonstrated the importance of the amygdala for fear conditioning [8–10]. Subsequent physiological experiments showed that learning produces prolonged synaptic modification in both of the inputs to the amygdala: the thalamo-amygdala pathway [11,12] and the cortico-amygdala pathway [13]. Evidence from many studies suggests that the amygdala—in particular, the lateral/basolateral nuclei—plays an essential role in the acquisition, storage and expression of fear memory [1,7,14–18].

Here, we developed an inducible striatal neuron ablation system in transgenic mice and examined the effect of striatal neuron ablation on auditory fear conditioning with different intensities of US. Under the standard condition, the ablation of striatal neurons in the adult brain hardly affected the auditory fear conditioning in agreement with previous studies [18–22]. We found, however, that under a weak condition, the formation of long-term auditory fear memory but not short-term memory was impaired by the ablation of striatal neurons. Our results suggest the presence of two forms of auditory fear memories distinguished by the US intensity and by the requirement of striatal neurons. Our finding that striatal neuron ablation diminished the auditory fear conditioning only when the US was weak is intriguing since the striatum is supposed to play a role in incorporating the positive or negative value of information into the determination of behavioral responses.

Results

Generation of striatum-specific Cre mouse lines

The G-protein γ7 subunit mRNA is expressed predominantly in medium spiny neurons of the caudate-putamen (CP) and nucleus

accumbens (NAc) and neurons of the olfactory tubercle [23]. To develop a striatal neuron-specific gene manipulation system, we produced Gγ7-Cre and Gγ7-mCrePR mouse lines by inserting the gene encoding Cre recombinase or Cre recombinase-progesterone receptor fusing protein (CrePR) into the translational initiation site of the G-protein γ7 subunit gene (*Gng7*) through homologous recombination in embryonic stem cells derived from the C57BL/6 strain [24] (Fig. 1A). We then crossed the Gγ7-Cre and Gγ7-mCrePR mice with the CAG-CAT-Z11 reporter mouse [25]. Brain slices prepared from Gγ7-Cre×CAG-CAT-Z11 mice were stained for β-galactosidase activity to monitor the Cre recombinase activity. Strong β-galactosidase staining was found predominantly in the CP, NAc and olfactory tubercle. Faint signals were detected in the layer 5 of the neocortex and subiculum (Fig. 1B). On the other hand, no β-galactosidase staining was detectable in brain slices from Gγ7-mCrePR×CAG-CAT-Z11 mice upon induction of Cre recombinase activity by RU-486 administration.

Inducible ablation of striatal neurons

We then crossed the Gγ7-mCrePR mouse with a knock-in mouse (Eno2-STOP-DTA) in which the Cre-inducible diphtheria toxin A gene (*DTA*) was introduced into the neuron-specific enolase gene (*Eno2*) locus [26]. In $Gng7^{+/mCrePR}$ mice, one allele retains the intact *Gng7* gene, and the other is inactivated by insertion of the *CrePR* gene. We injected 1 mg per g body weight of RU-486 into the peritoneum of Gγ7-mCrePR×Eno2-STOP-DTA mice at postnatal day 42 (P42) to induce the recombinase activity of CrePR [24,25,27] (Fig. 2A). Mock-injected mice served as controls. Ten days after RU-486 injection, TUNEL staining showed strong signals throughout the striatum, including the CP, NAc and olfactory tubercle (Fig. 2B). On the other hand, no TUNEL-signals were detectable in the striatum of the mock-injected mice. Both RU-486- and mock-treated mice showed faint TUNEL-signals in the olfactory bulb probably due to the turnover of adult-generated olfactory granule cells [28]. In addition, Gγ7-mCrePR mice exhibited no detectable TUNEL signals in the striatum upon RU-486 injection (data not shown). These results suggest that RU-486 treatment successfully induced recombination by CrePR, leading to cell ablation in the adult brain in the striatum-specific manner. Gγ7-CrePR-mediated recombination appeared to be critically dependent on target mice since β-galactosidase staining was hardly detectable in Gγ7-mCrePR× CAG-CAT-Z11 mice upon induction.

Thirteen days after RU-486 treatment, TUNEL signals in the striatum became undetectable in Gγ7-mCrePR×Eno2-STOP-DTA mice. We then quantitatively examined the ablation of striatal neurons by immunohistochemical staining for NeuN, a marker protein for neurons. The density of NeuN-positive neurons in the CP drastically decreased by 13 days after RU-486 injection ($F_{6,54} = 99.5$, $P<0.001$, one-way ANOVA) and remained at a very low level thereafter (Fig. 3A–C). The number of NeuN-positive cells in the NAc core and shell also decreased with a similar time course (Fig. 3B,D). However, NeuN immunostaining signals in other brain regions including the amygdala were comparable between mock- and RU-486-treated mice (Fig. 3B,E).

Medium-spiny projection neurons, the main output neurons, account for up to 90% of neurons in the striatum [29,30]. There were no detectable immunoreactivities for calbindin, a marker for medium-sized spiny neurons [31], in the mutant striatum (Fig. 4A). Medium-spiny projection neurons in the striatum can be largely subdivided into two groups: some that project to directly to the substantia nigra pars reticulata (SNr) (the direct pathway) express substance P; others that project to the same nucleus via the globus pallidus (GP) (the indirect pathway) express enkephalin [29]. These two neuropeptides are anterogradely transported to the axon terminals in the afferent regions [32]. There were no detectable immunoreactivities for substance P and enkephalin in

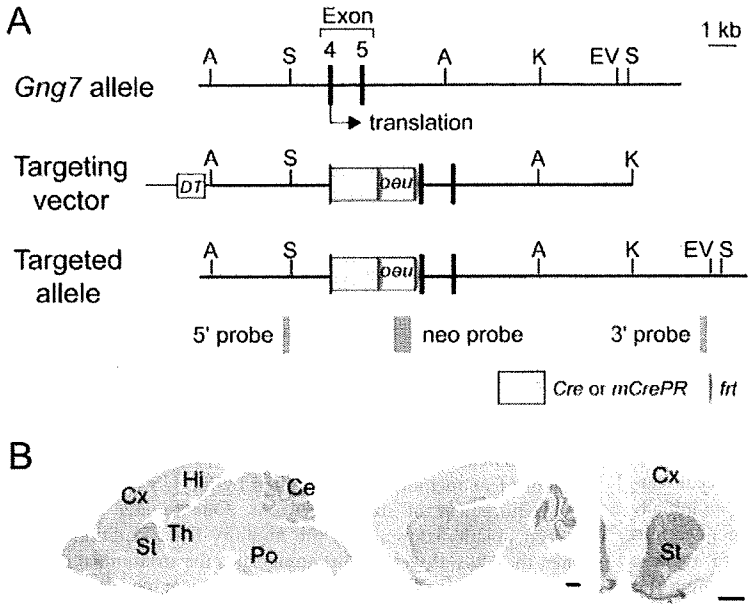

Figure 1. Generation of Gγ7-Cre and Gγ7-mCrePR mice. A, Schema of the exon 4 region containing the translational initiation site of the *Gng7* gene, targeting vector, and targeted allele. The targeting vector carries the *cre* or *mCrePR* gene and the *neo* gene flanked by two *frt* sequences. A, *ApaI*; EV, *EcoRV*; K, *KpnI*; S, *SpeI*. **B**, *LacZ* expression following Cre recombination. X-gal-staining of sagittal and coronal sections from $Gng7^{+/cre}$; +/*CAG-CAT-Z* mice at postnatal day 14. Sections were counterstained with nuclear fast red. Abbreviations: Ce, cerebellum; Cx, cortex; Hi, hippocampus; Po, pons; St, striatum; Th, thalamus. Scale bars, 1 mm.
doi:10.1371/journal.pone.0004157.g001

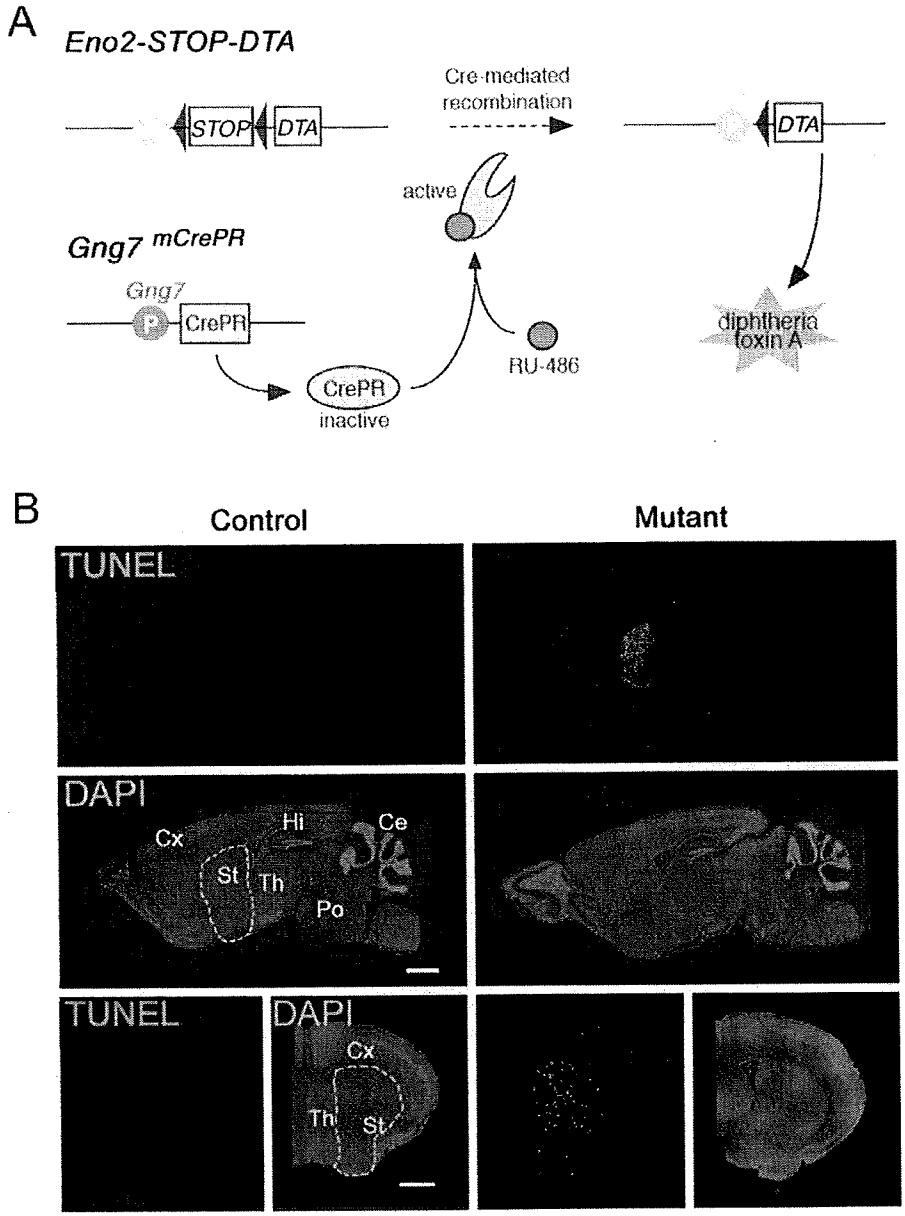

Figure 2. Inducible ablation of striatal neurons. A, Schema for striatal neuron ablation induced by RU-486 administration. **B**, TUNEL staining (green) counterstained with DAPI (blue) in brain sections of control (left) and mutant (right) mice 10 days after mock and RU-486 administration, respectively. Scale bars, 1 mm. Abbreviations: Ce, cerebellum; Cx, cortex; Hi, hippocampus; Po, pons; St, striatum; Th, thalamus.
doi:10.1371/journal.pone.0004157.g002

SNr and GP, respectively, of RU-486-treated mice (Fig. 4B,C), suggesting that any striatal output scarcely remains in the basal ganglia of the mutant mice. Along with the NeuN-immunohistochemistry, our results suggest that induction of CrePR-mediated DTA expression by RU-486 injection successfully ablated almost completely the medium spiny neurons that comprise approximately 90% of the NeuN-positive striatal neurons within 13 days. In subsequent analyses, we used Gγ7-mCrePR×Eno2-STOP-DTA mice from 13 to 22 days after RU-486 administration as striatal neuron-ablated mutant mice and corresponding mock-injected littermates served as controls.

Motor activity

The striatum is intimately involved in motor control. The striatal neuron-ablated mutant mice showed no ataxic gait or tremor and could walk along a straight line as control did (control, $n = 4$; mutant, $n = 4$) (Fig. 5A). There was no significant difference in the performance in the stationary thin rod test [33] between mutant and control mice ($F_{1,15} = 1.38$, $P = 0.26$, repeated measures ANOVA) (Fig. 5C). Thus, the ablation of striatal neurons appeared to exert little effect on motor coordination under standard conditions at least for a week after loss of ~90% striatal neurons. In the accelerating rotarod test [34], both mutant and

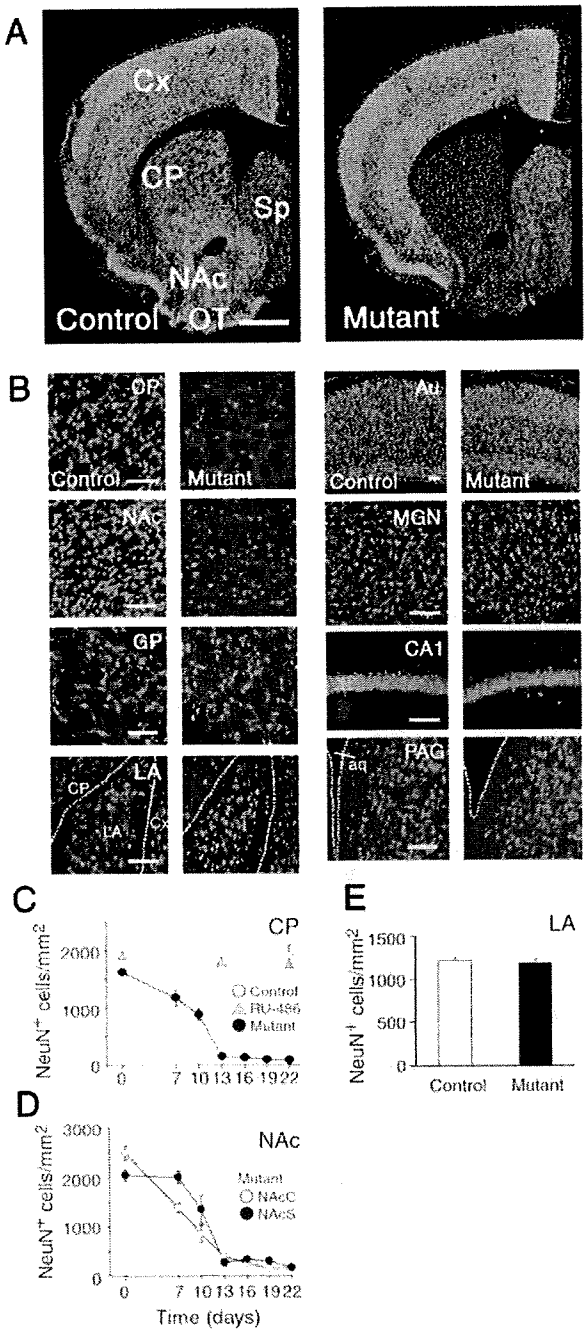

Figure 3. NeuN-immunohistochemstry. A, Immunohistochemical analysis for neuronal marker NeuN in control (left) and mutant (right) mice 13 days after mock and RU-486 administration, respectively. Scale bar, 1 mm. **B**, Higher magnification of NeuN-immunohistochemistry in various brain regions. Scale bars, 0.1 mm. **C**, NeuN immunoreactive ($NeuN^+$)-cell density in the CP after drug administration. $n=8$–9 each. **D**, Densities of NeuN-positive cells in the NAc core (NAcC, open circles) and the NAc shell (NAcS, filled circles) after RU-486 treatment of *Gng7*$^{+/mCrePR}$; *+/Eno2-STOP-DTA* mice ($n=8$–9 each). **E**, Densities of NeuN-positive cells in the lateral amygdala (LA) of control and mutant mice 22 days after mock and RU-486 treatment, respectively ($n=15$ each, $F_{1,28}=0.23$, $P=0.64$, one-way ANOVA). Abbreviations: Au, auditory cortex; CA1, hippocampal CA1 region; CP, caudate putamen; Cx, cortex; GP, globus pallidus; MGN, medial geniculate nucleus of thalamus; NAc, nucleus accumbens; OT, olfactory tubercle; PAG, periaqueductal gray; Sp, septum.
doi:10.1371/journal.pone.0004157.g003

control mice performed equally well in the first training session ($F_{1,14}=3.57$, $P=0.08$, one-way ANOVA) (Fig. 5D). Despite that approximately 90% of striatal neurons were ablated, the motor performance of the mutant mice appeared to be comparable to that of control mice in stationary thin rod and rotating rod tests. In subsequent sessions of the accelerating rotarod test, however, there was a significant difference in the retention time between two groups ($F_{1,14}=37.2$, $P<0.001$, repeated measures ANOVA). Control mice showed a steady and rapid improvement in their performance over the training. In contrast, mutant mice failed to exhibit any improvements over trials, suggesting that the striatal neurons are indispensable for motor learning. Our results are consistent with the observation that striatum-specific NMDA receptor mutant mice showed impaired motor learning in an accelerating rotarod test [35]. In the open field test, the locomotor activity of mutant mice tended to be higher than that of control mice ($F_{1,15}=4.6$, $P=0.05$) (Fig. 5E).

The degeneration of striatal neurons is associated with Huntington's disease [36,37] and dystonia [38,39]. Mutant mice, however, showed no abnormal clasping behavior induced by a tail suspension in a dystonic fashion ($n=6$) (Fig. 5B); the clasping behavior was observed in the mutant mice 6 weeks after RU-486 injection. In addition, there were no easily recognizable movement disorders in mutant mice at least for a week after the drug-induced ablation of striatal neurons had been completed.

Impairment of auditory fear conditioning with a low-intensity footshock

Mutant mice were subjected to auditory fear conditioning to examine the possible involvement of striatal neurons in the formation of the emotional memory. Fourteen days after RU-486 treatment, mutant mice were trained for auditory fear conditioning (Fig. 6A). Mice were given a single pairing of tone (CS) and footshock (US; 0.5 mA) on the conditioning day (Fig. 6B). Twenty-four hours after the conditioning, the mice were placed in a novel chamber. Six min after placement, the tone was delivered for 3 min. Mice exhibited a range of conditioned fear responses including freezing. Levels of freezing during the pre-tone period were comparable between mutant and control mice ($F_{1,15}=2.28$, $P=0.15$). Freezing responses to the tone were also similar between mutant and control mice (control, 31.6±5.1%; mutant, 28.0±5.1%; $F_{1,15}=0.27$, $P=0.61$) (Fig. 6B). Thus, mutant mice successfully acquired fear memory under the standard condition despite of almost complete ablation of striatal medium spiny neurons.

We further investigated the ability of mutant mice to acquire fear memory under a less intensive condition. Mice were trained with a single paring of the tone and a low-intensity footshock at 0.3 mA, and tested for the freezing response 24 h after training. Negligible levels of freezing were observed during the pre-tone period in control and mutant mice as well as RU-486-treated Gγ7-mCrePR mice (RU-486 control). However, there were significant differences in the freezing responses across the CS presentation among 3 groups of mice (control, 29.7±4.9%; RU-486 control, 31.5±4.9%; mutant, 13.6±2.7%; $F_{2,23}=6.57$, $P=0.006$) (Fig. 6C). The freezing levels of mutant mice were much lower than those of control mice ($P<0.05$, mutant vs. control; $P<0.01$, mutant vs. RU-486 control; Post-hoc analysis). Comparable levels of freezing between control and RU-486-control mice indicated that treatment of RU-486 itself exerted little effect on the fear conditioning. There were no significant differences among control, RU-486 control, and mutant mice in pain thresholds for flinch and jump reactions (flinch, $F_{2,16}=0.094$, $P=0.91$, one-way ANOVA; jump, $F_{2,16}=0.021$, $P=0.98$) (Fig. 6D). The post-shock activity bursts [40] of mutant and control mice were also similar (at

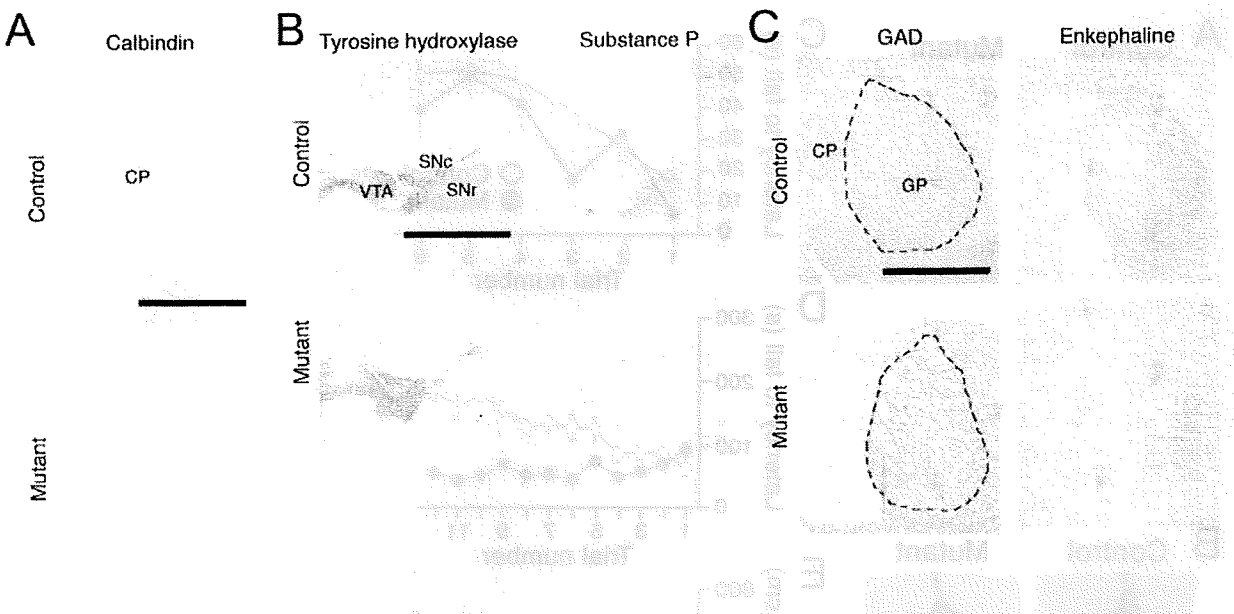

Figure 4. Ablation of medium-spiny projection neurons in the striatum of mutant mice. A, Immunoreactivity for calbindin in the dorsal striatum of control (upper) and mutant (lower) mice. **B**, Immunoreactivity for tyrosine hydroxylase and substance P in substantia nigra of control and mutant mice. **C**, Immunoreactivity for GAD and enkephalin in GP of control and mutant mice. Abbreviations: CP, caudate putamen; GP, globus pallidus; SNc, substantia nigra pars compacta; SNr, substantia nigra pars reticulata; VTA, ventral tegmental area. Scale bars, 1 mm.
doi:10.1371/journal.pone.0004157.g004

0.3 mA, $F_{2,31} = 3.30$, $P = 0.98$; at 0.5 mA, $F_{1,13} = 4.67$, $P = 0.23$). These results suggest that striatal neurons are indispensable for efficient auditory fear conditioning with the low-intensity US.

Impairment of long-term fear memory

To further examine the role of striatal neurons in fear conditioning, we trained mice under the weak condition (a single paring of tone and footshock at 0.3 mA), tested for short-term memory (STM) 1 or 3 h after training and then retested for long-term memory (LTM) 24 h after training [41] (Fig. 7A). The freezing responses of mutant mice were comparable to those of control mice 1 h after conditioning (control, 19.7±3.0%; mutant, 34.5±7.2%; $F_{1,11} = 3.20$, $P = 0.10$, repeated measures ANOVA) (Fig. 7B left panel) as well as 3 h after conditioning (control, 20.6±3.6%; mutant, 24.2±7.1%; $F_{1,8} = 0.51$, $P = 0.50$) (Fig. 7C left panel). Twenty-four hours after training, however, mutant mice showed significantly smaller freezing responses than control mice (Fig. 7B right panel, control, 28.0±4.6%; mutant, 3.4±1.8%; $F_{1,11} = 8.06$, $P = 0.02$: Fig. 7C right panel, control, 17.7±4.0%; mutant, 2.9±1.2%; $F_{1,8} = 46.7$, $P < 0.001$). These results suggest that the striatal neurons are involved selectively in the acquisition of LTM under the weak conditioning, but not in that of STM. The intact STM formation in mutant mice is consistent with no detectable alterations in the sensitivity to the electric footshock as above.

Impairment of fear memory retention

We further examined whether the ablation of striatal neurons affects the retention of previously acquired fear memory (Fig. 7D). Mice were first trained with a single paring of tone and footshock at 0.3 mA and placed back in the home cage. Twenty-four hours after conditioning when LTM was formed, the animals were treated with RU-486 for induction of striatal neuron ablation. When tested 14 days after the drug treatment, RU-486-injected mice showed significantly smaller freezing responses during tone presentation than mock-injected mice (mock-injected mice, 37.6±3.9%; RU-486-injected mice, 11.5±2.6%; $F_{1,13} = 41.9$, $P < 0.001$) (Fig. 7E). On the other hand, the ability of RU-486-injected mice to retain the acquired fear memory under the standard condition (0.5 mA) was comparable to that of mock-injected mice (mock-injected mice, 50.1±6.8%; RU-486-injected mice, 40.8±8.0%; $F_{1,11} = 0.32$, $P = 0.58$) (Fig. 7F), consistent with the observation that pre-conditioning ablation of striatal neurons hardly affected the auditory fear conditioning (Fig. 6B). These results suggest that the striatal neurons are required for the retention of fear memory previously acquired by the conditioning with the low-intensity US.

Discussion

Here, we show that striatal neurons can be selectively ablated upon induction in mice carrying *Gng7*-promoter-driven *CrePR* and Cre-dependent *DTA* genes. Despite that approximately 90% of striatal neurons were ablated, the motor performance of the mutant mice appeared to be comparable to that of control mice in stationary thin rod and rotating rod tests. However, the improvement of the mutant mice in the performance over trials was impaired in the accelerating rotarod test, suggesting the requirement of striatal neurons for motor learning. In addition, the mutant mice showed no abnormal behavior in the tail suspension test and there were no easily recognizable movement disorders in the mutant mice at least for a week after the drug-induced ablation of striatal neurons had been completed. Interestingly, however, the clasping behavior was observed 6 weeks after RU-486 injection. The motor phenotypes of mutant mice appeared later might be caused by secondary changes of the brain. It is known that dystonic symptoms occur a long time after brain injury, suggesting secondary changes [42,43].

One to several pairings of tones with footshocks at 0.5–2 mA are generally used for fear conditioning in rodents [18–22]. The

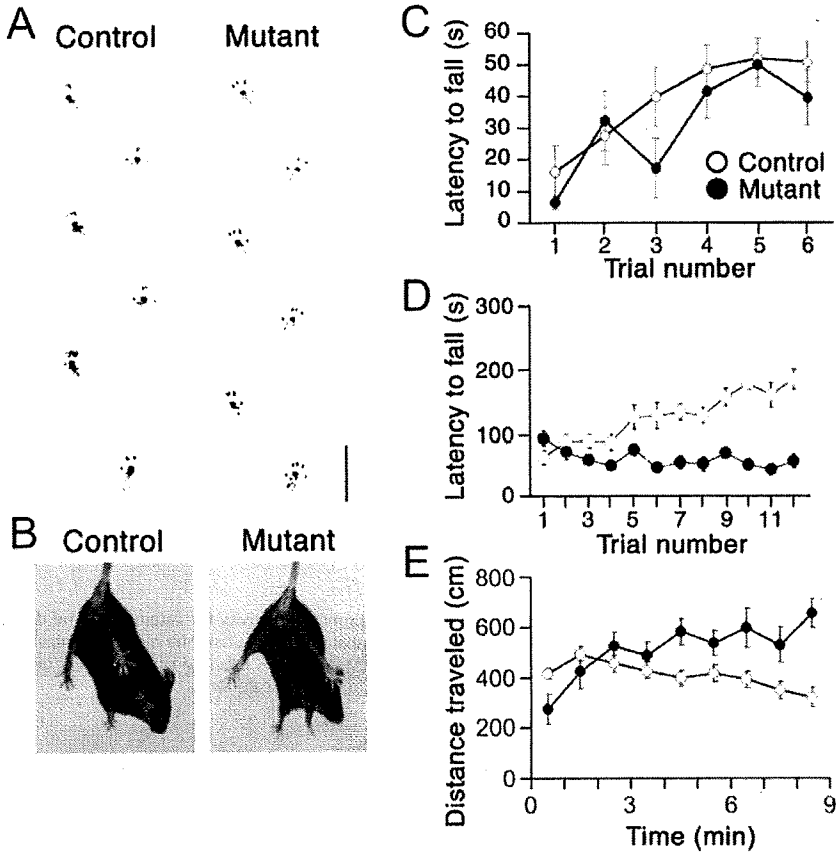

Figure 5. Performance of mutant mice in motor tests. A, Foot print of control (left) and mutant (right) mice. Scale bar, 2 cm. **B,** Tail suspension test of control (left) and mutant (right) mice. **C,** Performance of control (open circles, $n=9$) and mutant (filled circles, $n=8$) mice in the stationary thin rod test. **D,** Performance of control (open circles) and mutant (filled circles) mice in the accelerating rotarod ($n=8$ each). **E,** Locomotor activity of control (open circles, $n=10$) and mutant (filled circles, $n=7$) mice in the openfield test.
doi:10.1371/journal.pone.0004157.g005

striatal neuron ablation hardly affected the auditory fear conditioning with a single pairing of tone with the footshock at 0.5 mA. Our results are consistent with previous ones that electrolytic or excitotoxic lesion of the striatum exerted little effect on the auditory fear conditioning [19–21]. On the other hand, a slight impairment of fear conditioning with 5 tone-footshock (0.5–1 mA) pairings was reported for dorsal striatum- or NAc shell-lesioned rats [44,45]. It will be difficult to ascertain whether the discrepant behavioral effects of classical lesion studies were caused by ablation of striatal neurons or other impairments. Our genetic ablation system specific for striatal neurons provides evidence supporting the view that the amygdala but not the striatum is essential for the auditory fear conditioning under the standard condition.

In the present investigation, we found that when the tone was paired with the low-intensity footshock at 0.3 mA, the freezing responses 24 h after conditioning were significantly reduced in the striatal neuron-ablated mice. The impairment of tone-dependent fear conditioning with the low-intensity US itself does not reveal a specific role of these striatal neurons in either the learning or the performance of conditioned fear. However, the observation that the freezing responses of the mutant mice measured 1 h or 3 h after conditioning with the low-intensity US were comparable with those of control mice excluded the possibility that the striatal neuron ablation simply disrupted the animal's ability to make the freezing responses. Furthermore, the mutant mice showed the ability to acquire, retain and express the cued fear memory at least for 3 h after conditioning with the low-intensity US. It is to be noted with this respect that the induction of cell ablation was selective for striatal neurons, leaving the amygdala intact, which plays an essential role in the acquisition, storage and expression of fear memory [2,18,20]. Thus, the striatal neuron ablation appeared to impair the formation and/or retention of long-term fear memory rather than performance or acquisition and expression of fear memory. Consistently with this possibility, the ablation of striatal neurons after long-term fear memory formation, that is, 24 h after conditioning with the low-intensity US, diminished the retention of the LTM.

These results obtained by the use of an inducible striatal neuron-ablation system suggest the presence of at least two forms of the auditory fear memories distinguished by the US intensity and by the requirement of striatal neurons. Under the standard condition, auditory fear memory formation is hardly affected by the striatal neuron ablation, in agreement with previous studies showing that the amygdala but not the striatum plays a central role in the auditory fear conditioning [2,18–21]. When auditory fear conditioning was carried out with the low-intensity US, the formation of LTM but not STM became sensitive to striatal

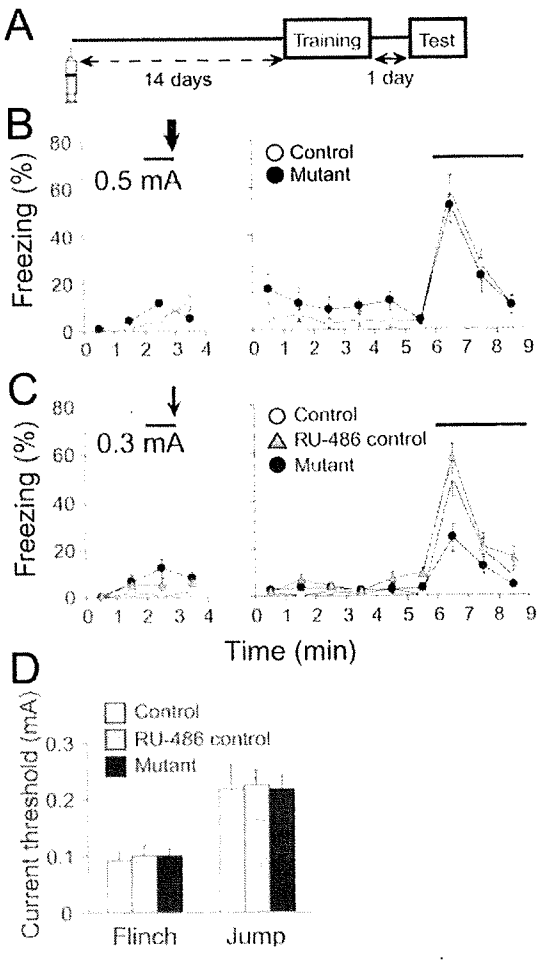

Figure 6. Impaired freezing responses of mutant mice after auditory fear conditioning with a low-intensity footshock. A, Experimental design. Mice were injected with RU-486 or vehicle. Fourteen days after treatment, the animals were subjected to auditory fear conditioning. **B,** Freezing responses of control (open circles, $n=9$) and mutant (filled circles, $n=8$) mice on the conditioning (left) and test (right) days. Auditory fear conditioning was carried out with the standard intensity of footshock (0.5 mA, an arrow). Solid lines represent tone. **C,** Freezing responses of control (open circles, $n=8$) and mutant (filled circles, $n=11$) mice and RU-486-treated Gγ7-mCrePR mice (RU-486 control) (shaded triangles, $n=7$) on the conditioning (left) and test (right) days. Auditory fear conditioning was carried out with a low intensity of footshock (0.3 mA, an arrow). Solid lines represent tone. **D,** Current thresholds of control (open bar), RU-486-control (shaded bar) and mutant (filled bar) mice for flinch and jump reactions ($n=6$ each).
doi:10.1371/journal.pone.0004157.g006

neuron ablation. Thus, our results reveal a novel form of the auditory fear memory depending on striatal neurons at the low-intensity US. When the US becomes weaker, it will be less threatening and more difficult to judge whether it is dangerous enough to be memorized for animals. Our finding that striatal neuron ablation diminished the auditory fear conditioning only when a footshock was weak is of interest in view that the striatum is supposed to play a role in incorporating the positive or negative value of information into the determination of behavioral responses [46–48]. It is possible, though not proven, that striatal neurons may be activated by the weak US and directly or indirectly involved in the consolidation or retrieval of the long-term fear memory. While the contextual fear conditioning requires the hippocampus and amygdala, our results suggest further integration of brain systems for the emotional memory by showing the involvement of the striatum in the auditory fear conditioning at the weak US. Fear is an adaptive component of response to potentially threatening stimuli, but too much or inappropriate fear accounts for many common psychiatric problems, such as anxiety disorders [3–5]. Advances in basic and clinical neuroscience studies of fear are important for the development of strategies to treat and cure anxiety disorders [49,50]. Thus, the finding of a novel form of the auditory fear memory might have therapeutic implications.

Materials and Methods

Generation of striatum-specific Cre mice

A full-length cDNA (210 bp) encoding the mouse G-protein γ7 subunit was amplified with primers 5′-GATGTCAGGTACTAA-CAACGTCGCCC-3′ and 5′-CTAGAGAATTATGCAAGGC-TTTTTGTCTTT-3′ from a brain cDNA library from ICR mice. Using the cDNA fragment as a probe, we isolated a BAC clone containing the exon 4 and 5 of the *Gng7* by screening a genomic DNA library of C57BL/6 mouse (Genome systems, St. Louis, MO). The 8.9 kb-*Spe*I-*Kpn*I fragment from the BAC clone was inserted into the *Spe*I-*Kpn*I sites of pBluescript II SK(+) (Stratagene, La Jolla, CA) to yield pGng7MET. The 523 bp *Eco*RI-*Age*I fragment generated by 2-step-PCR using pGng7MET and pNCre [25] as templates and the 989 bp *Age*I-*Eco*RI fragment from pNCre were cloned into the *Eco*RI site of pBluescript II SK(+) to yield pGng7Cre. The 1.4 kb *Eco*RI-*Sac*I fragment from pGK1NeopA [27] was blunted and inserted into the *Eco*RV site of pGng7Cre to yield pCreNeo. Synthetic oligonucleotides (5′-AGCTTTCAGGTACTAACAACGTCGCCCAGGCCCGGA-AGCTGGTGGAGCAGC-3′ and 5′-GCAGCTGCTCCACCA-GCTTCCGGGCCTGGGCGACGTTCTTAGTACCTGAA-3′) and the 7.5 kb *Fsp*I-*Kpn*I fragment from pGngMET were ligated with the *Hind*III (blunted)- and *Kpn*I-digested pBluescript II SK(+) to yield pFSKP. The 7.5 kb *Eco*RV-*Kpn*I fragment from pFSKP was ligated with the *Hind*III (blunted)- and *Kpn*I-digested pCreNeo to yield pBTV. *Kpn*I-digested pMC1DTApA was blunted and ligated, and the 4.3 kb *Not*I-*Hind*III fragment from the resulting plasmid was ligated with synthetic oligonucleotides, 5′-GGCCGCGGTACCCGGGTCGACTTA-3′ and 5′-AGCT-TAAGTCGACCCGGGTACCGC-3′, to yield pMC1DTApA2. The 11.1 kb *Not*I-*Kpn*I fragment of pBTV was inserted into the *Not*I-*Kpn*I sites of pMC1DTpA2 to yield targeting vector pGng7CreTV. The Cre coding sequence of the *CrePR* gene [25,27] was replaced by that of mammalian Cre with the optimal codon usage in mammals by 2-step PCR using pNCrePR [25] and pCXN-Cre [51]. The 1.9-kb fragment encoding mammalian CrePR (mCrePR) was cloned into the *Xba*I site of pEF-BOS [52] to yield pmNCrePR. The *cre* gene in pGngCreTV was replaced by the *mCrePR* gene to yield targeting vector pGngmCrePRTV.

The targeting vectors were linearized by *Kpn*I and electroporated into ES cells derived from the C57BL/6 strain [24,27]. Recombinant clones were identified by Southern blot analysis of genomic DNA using 0.25 kb *Age*I-*Spe*I fragment from the BAC clone, 0.6 kb-*Pst*I-*Pst*I fragment from pPGK1-NeopA and 0.3 kb *Nde*I-*Sac*I fragment from the BAC clone as 5′ outer, neo, and 3′ outer probes, respectively. Chimeric mice production was carried out essentially as described [24,27]. The $Gng7^{Cre}$ allele was identified by PCR using primers CreP1 and CreP2 [25]. The

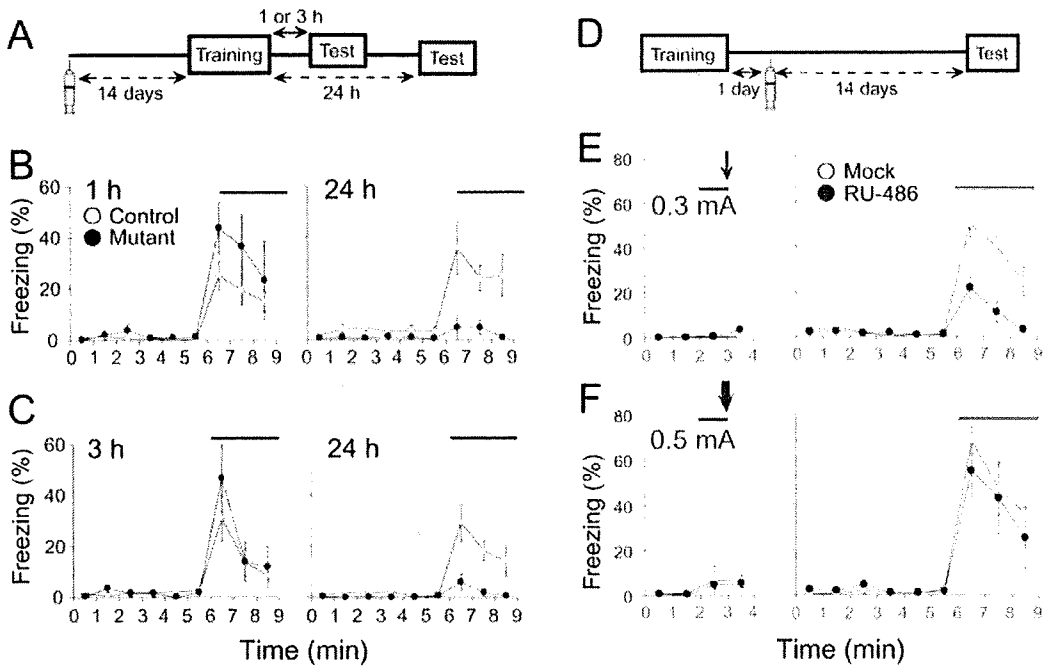

Figure 7. Impairment of long-term fear memory. A, Experimental design. Mice were injected with RU-486 or vehicle. Fourteen days after treatment, the animals were subjected to auditory fear conditioning with a weak footshock at 0.3 mA. Freezing responses to tone were measured 1 or 3 h and 24 h after conditioning. **B**, Freezing responses of control (open circles, $n=8$) and mutant (filled circles, $n=5$) mice 1 h (left) and 24 h (right) after conditioning. **C**, Freezing responses of control (open circles, $n=6$) and mutant (filled circles, $n=4$) 3 h (left) and 24 h (right) after conditioning. **D**, Experimental design. Mice were subjected to auditory fear conditioning with a footshock at 0.3 mA or 0.5 mA. One day after conditioning, the conditioned mice were injected with RU-486 or vehicle. Their freezing responses were measured 14 days after drug treatment. **E**, Mice were subjected to auditory fear conditioning with a weak footshock at 0.3 mA. Freezing responses of mock-injected (open circles, $n=7$) and RU-486-injected (filled circles, $n=8$) mice on the conditioning (left) and test (right) days. **F**, Mice were subjected to auditory fear conditioning with the standard footshock at 0.5 mA. Freezing responses of mock-injected (open circles, $n=6$) and RU-486-injected (filled circles, $n=7$) mice on the conditioning (left) and test (right) days.
doi:10.1371/journal.pone.0004157.g007

Gng7^{mCrePR} allele was identified by PCR using primers 5′-TATAGGTACCCAGAAGTGAATTCGGTTCGC-3′, 5′-GGCGACGTTGTTAGTACCTGAC-3′ and 5′-GTGCAGCATGTTCAGCTGGC-3′.

Eno2-STOP-DTA mouse [26] was backcrossed 7 times to the C57BL/6 strain. The *Eno2-STOP-DTA* allele was identified by PCR using primers 5′-AATTCTTAATTAAGGCGCGCGGG-3′, 5′-GTCAGAATTGAGGAAGAGCTGGGG-3′ and 5′-CACTGAGGATTCTTCTGTGG-3′. Breeding and maintenance of mice were carried out under institutional guidelines. Mice were fed *ad libitum* with standard laboratory chow and water in standard animal cages under a 12 h light/dark cycle. All animal procedures were approved by the Animal Care and the Use Committee of Graduate School of Medicine, the University of Tokyo (Approval #1721T062).

Induction of CrePR recombinase activity

RU-486 (Sigma, St. Louis, MO) was suspended at a concentration of 50 mg/ml in water containing 0.25% carboxymethyl cellulose (Sigma) and 0.5% Tween 80 (Sigma). We injected 1 mg per g body weight of RU-486 into the peritoneum of mice at P42.

Histochemistry

Under deep pentobarbital anesthesia (100 mg/kg), animals were perfused transcardially with 4% paraformaldehyde in 0.1 M phosphate buffered salts (PBS). β-Galactosidase staining was conducted as described previously [25]. Immunohistochemistry was performed as described previously [27] using antibodies against neuronal nuclei (NeuN), enkephalin, glutamic acid decarboxylase (GAD), substance P (Chemicon International, Temecula, CA), tyrosine hydroxyrase (Santacruz Biotechnology, Santa Cruz, CA), and calbindin. The numbers of NeuN-positive cells per 8.7×10^{-2} mm^2 were counted at the dorsolateral part of CP, dorsomedial part of NAc core, the medial part of the NAc shell (AP = 1.2 mm from bregma), and the LA (AP = −1.7 mm) in the coronal brain sections. Only unequivocally stained cells were counted using the ImageJ software by two observers blind to the origin of the sections.

Terminal deoxynucleotidyl transferase-mediated dUTP nick-end labeling (TUNEL) histochemistry was performed using ApopTag Fluorescein Direct In Situ Apoptosis Detection Kit (Chemicon International) according to the instructions of the manufacturer. In brief, sections were incubated in PBS containing 20 μg/ml proteinase K (Ambion, Austin, TX) at room temperature for 15 min, washed and stained using FITC-labeled dUTP and terminal deoxynucleotide transferase (TdT) (Chemicon International) at 37°C for 60 min. After TUNEL reaction was terminated, slides were mounted using Vectashield H-1500 mounting solution that contains DAPI (Vector, Burlingame, CA). Confocal images were obtained using confocal microscopes (TCS-SP5, Leica, Wetzlar, Germany).

Fear conditioning

A computer-controlled fear conditioning system (CL-M2; O'Hara, Tokyo, Japan) was used in the fear conditioning

experiments. A clear conditioning chamber (10×10×10 cm) with polyvinyl chloride boards and a stainless steel rod floor that was composed of 14 stainless steel rods (2 mm in diameter spaced 7 mm apart) was surrounded by a sound-attenuating white chest (74 lux). Masking noise of 52 dB was provided by a ventilation fan. Mice were housed individually for 1 week before behavioral testing and were handled for 30 s everyday. On the conditioning day, mice were placed in the conditioning chamber for 2 min and then presented with a loud tone (65 dB, 10 kHz) for 1 min through a speaker on the ceiling of the conditioning chest. At the end of the tone presentation, the mice were given a scrambled electrical footshock (0.3 mA or 0.5 mA for 1 s). One minute after footshock, the mice were returned to their home cages. The conditioning chamber was cleaned with 70% ethanol between sessions. On the test day, mice were placed in a novel translucent acryl chamber with paper chips surrounded by a sound-attenuating black chest for 6 min and subsequently for 3 min in the presence of the tone. The test chamber was cleaned with benzalkonium (Ecolab, St. Paul, MN) between tests. All behaviors were monitored by a CCD camera (WAT-902B; Watec, Yamagata, Japan) attached to the ceiling of the chest. Eight bit grayscale images (90×90 pixels) were captured at a rate of two frames per second and freezing behavior was automatically analyzed as an index of fear using IMAGE FZC software (O'Hara). Freezing behavior was defined as the absence of any visible movement of the body and vibrissae except for movement necessitated by respiration. Freezing time was summated and the percentage of freezing was calculated per minute. To examine pain sensitivity, we measured current thresholds for reactions of mice to nociceptive shock, namely, flinch and jump [53]. Mice were given footshocks of increasing strength ranging from 0.05 to 0.5 mA in a stepwise manner by 0.05 mA with an interval of 30 s.

Motor behaviors

The stationary horizontal thin rod test was done as described [33]. The rod was 15 mm in diameter and 50 cm long and placed 40 cm high to discourage jumping. A mouse was placed on the midpoint of the rod, and the time it remained on the rod was measured; animals staying for 60 sec were taken from the rod and recorded as 60 s. Six consecutive trials were performed with an intertrial interval of 1 h.

The accelerating rotarod test was performed with an apparatus consisted of a 3.2 cm-diameter rod (RRAC-3002; O'Hara & Co., Tokyo, Japan) essentially as described [34]. During the training period, mice were placed on the rotating rod starting at 5 rpm and gradually accelerated to 50 rpm at a rate 0.15 rpm/s. The latency to fall (retention time) was measured with cutoff time of 5 min. Mice were trained for 3 consecutive days, receiving 4 trials per day with an intertrial interval of 1 h.

In the tail suspension test [54], mice were observed for 15 s. Abnormal movement was defined as any dystonic movement of the hindlimbs, forelimbs, or trunk with full clasping where limbs were pulled into the central body axis.

In the open field test, locomotor activity was measured for 9 min in a square chamber (50×50×40 cm) with a CCD camera on the ceiling (OF4, O'Hara). Images were captured at a rate of one frame per second and walking distance was automatically measured by IMAGE OF4 software (O'Hara).

Statistics

Data are expressed as mean±SEM. The statistics significance was evaluated using one-way or repeated measures ANOVA. When the interaction was significant, Fisher's PLSD post hoc test was employed. The criterion for statistical significance was $P<0.05$.

Acknowledgments

We thank Ms. R. Natsume for chimeric mouse preparation, Dr. S. Miyagawa for providing pCXN-Cre and Dr. M. Tsujita for the construction of pEF-mNCrePR.

Author Contributions

Conceived and designed the experiments: MM. Performed the experiments: AK FF TI HK. Analyzed the data: AK FF TI. Contributed reagents/materials/analysis tools: HK HM TI SI KS. Wrote the paper: AK FF MM.

References

1. Davis M (1992) The role of the amygdala in fear and anxiety. Annu Rev Neurosci 15: 353–375.
2. LeDoux JE (2000) Emotion circuits in the brain. Annu Rev Neurosci 23: 155–184.
3. Kent JM, Rauch SL (2003) Neurocircuitry of anxiety disorders. Curr Psychiatry Rep 5: 266–273.
4. Millan MJ (2003) The neurobiology and control of anxious states. Prog Neurobiol 70: 83–244.
5. Uys JD, Stein DJ, Daniels WM, Harvey BH (2003) Animal models of anxiety disorders. Curr Psychiatry Rep 5: 274–281.
6. Blanchard RJ, Yudko EB, Rodgers RJ, Blanchard DC (1993) Defense system psychopharmacology: an ethological approach to the pharmacology of fear and anxiety. Behav Brain Res 58: 155–165.
7. LeDoux JE (1996) The emotional brain: the mysterious underpinnings of emotional life. New York: Simon & Schuster. 384 p.
8. Armony JL, Quirk GJ, LeDoux JE (1998) Differential effects of amygdala lesions on early and late plastic components of auditory cortex spike trains during fear conditioning. J Neurosci 18: 2592–2601.
9. Kapp BS, Frysinger RC, Gallagher M, Haselton JR (1979) Amygdala central nucleus lesions: effect on heart rate conditioning in the rabbit. Physiol Behav 23: 1109–1117.
10. LeDoux JE, Sakaguchi A, Reis DJ (1984) Subcortical efferent projections of the medial geniculate nucleus mediate emotional responses conditioned to acoustic stimuli. J Neurosci 4: 683–698.
11. McKernan MG, Shinnick-Gallagher P (1997) Fear conditioning induces a lasting potentiation of synaptic currents in vitro. Nature 390: 607–611.
12. Rogan MT, Staubli UV, LeDoux JE (1997) Fear conditioning induces associative long-term potentiation in the amygdala. Nature 390: 604–607.
13. Tsvetkov E, Carlezon WA, Benes FM, Kandel ER, Bolshakov VY (2002) Fear conditioning occludes LTP-induced presynaptic enhancement of synaptic transmission in the cortical pathway to the lateral amygdala. Neuron 34: 289–300.
14. Fanselow MS, LeDoux JE (1999) Why we think plasticity underlying Pavlovian fear conditioning occurs in the basolateral amygdala. Neuron 23: 229–232.
15. Fendt M, Fanselow MS (1999) The neuroanatomical and neurochemical basis of conditioned fear. Neurosci Biobehav Rev 23: 743–760.
16. Maren S (2001) Neurobiology of Pavlovian fear conditioning. Annu Rev Neurosci 24: 897–931.
17. Maren S, Fanselow MS (1996) The amygdala and fear conditioning: has the nut been cracked? Neuron 16: 237–240.
18. Maren S, Quirk GJ (2004) Neuronal signalling of fear memory. Nat Rev Neurosci 5: 844–852.
19. Haralambous T, Westbrook RF (1999) An infusion of bupivacaine into the nucleus accumbens disrupts the acquisition but not the expression of contextual fear conditioning. Behav Neurosci 113: 925–940.
20. LeDoux JE, Cicchetti P, Xagoraris A, Romanski LM (1990) The lateral amygdaloid nucleus: sensory interface of the amygdala in fear conditioning. J Neurosci 10: 1062–1069.
21. Riedel G, Harrington NR, Hall G, Macphail EM (1997) Nucleus accumbens lesions impair context, but not cue, conditioning in rats. Neuroreport 8: 2477–2481.
22. Romanski LM, LeDoux JE (1992) Equipotentiality of thalamo-amygdala and thalamo-cortico-amygdala circuits in auditory fear conditioning. J Neurosci 12: 4501–4509.
23. Watson JB, Coulter PM 2nd, Margulies JE, de Lecea L, Danielson PE, et al. (1994) G-protein γ7 subunit is selectively expressed in medium-sized neurons and dendrites of the rat neostriatum. J Neurosci Res 39: 108–116.
24. Mishina M, Sakimura K (2007) Conditional gene targeting on the pure C57BL/6 genetic background. Neurosci Res 58: 105–112.

25. Tsujita M, Mori H, Watanabe M, Suzuki M, Miyazaki J, et al. (1999) Cerebellar granule cell-specific and inducible expression of Cre recombinase in the mouse. J Neurosci 19: 10318–10323.
26. Kobayakawa K, Kobayakawa R, Matsumoto H, Oka Y, Imai T, et al. (2007) Innate versus learned odour processing in the mouse olfactory bulb. Nature 450: 503–508.
27. Takeuchi T, Miyazaki T, Watanabe M, Mori H, Sakimura K, et al. (2005) Control of synaptic connection by glutamate receptor δ2 in the adult cerebellum. J Neurosci 25: 2146–2156.
28. Biebl M, Cooper CM, Winkler J, Kuhn HG (2000) Analysis of neurogenesis and programmed cell death reveals a self-renewing capacity in the adult rat brain. Neurosci Lett 291: 17–20.
29. Gerfen CR, Engber TM, Mahan LC, Susel Z, Chase TN, et al. (1990) D1 and D2 dopamine receptor-regulated gene expression of striatonigral and striatopallidal neurons. Science 250: 1429–1432.
30. Graveland GA, DiFiglia M (1985) The frequency and distribution of medium-sized neurons with indented nuclei in the primate and rodent neostriatum. Brain Res 327: 307–311.
31. Xu M, Moratalla R, Gold LH, Hiroi N, Koob GF, et al. (1994) Dopamine D1 receptor mutant mice are deficient in striatal expression of dynorphin and in dopamine-mediated behavioral responses. Cell 79: 729–742.
32. Drago J, Padungchaichot P, Wong JY, Lawrence AJ, McManus JF, et al. (1998) Targeted expression of a toxin gene to D1 dopamine receptor neurons by cre-mediated site-specific recombination. J Neurosci 18: 9845–9857.
33. Airaksinen MS, Eilers J, Garaschuk O, Thoenen H, Konnerth A, et al. (1997) Ataxia and altered dendritic calcium signaling in mice carrying a targeted null mutation of the calbindin D28k gene. Proc Natl Acad Sci U S A 94: 1488–1493.
34. Nolan MF, Malleret G, Lee KH, Gibbs E, Dudman JT, et al. (2003) The hyperpolarization-activated HCN1 channel is important for motor learning and neuronal integration by cerebellar Purkinje cells. Cell 115: 551–564.
35. Dang MT, Yokoi F, Yin HH, Lovinger DM, Wang Y, et al. (2006) Disrupted motor learning and long-term synaptic plasticity in mice lacking NMDAR1 in the striatum. Proc Natl Acad Sci U S A 103: 15254–15259.
36. Albin RL, Young AB, Penney JB (1989) The functional anatomy of basal ganglia disorders. Trends Neurosci 12: 366–375.
37. Ferrante RJ, Kowall NW, Beal MF, Richardson EP Jr, Bird ED, et al. (1985) Selective sparing of a class of striatal neurons in Huntington's disease. Science 230: 561–563.
38. Rothwell JC, Obeso JA (1987) The anatomical and physiological basis of torsion dystonia. Marsden CD, Fahn S, eds. London: Butterworths. 468 p.
39. Waters CH, Faust PL, Powers J, Vinters H, Moskowitz C, et al. (1993) Neuropathology of lubag (X-linked dystonia parkinsonism). Mov Disord 8: 387–390.
40. Fanselow MS (1984) Opiate modulation of the active and inactive components of the postshock reaction: Parallels between naloxone pretreatment and shock intensity. Behav Neurosci 98: 269–277.
41. Bourtchuladze R, Frenguelli B, Blendy J, Cioffi D, Schutz G, et al. (1994) Deficient long-term memory in mice with a targeted mutation of the cAMP-responsive element-binding protein. Cell 79: 59–68.
42. Schoenfeld TA, Hamilton LW (1977) Secondary brain changes following lesions: A new paradigm for lesion experimentation. Physiol Behav 18: 951–967.
43. Breakefield XO, Blood AJ, Li Y, Hallett M, Hanson PI, et al. (2008) The pathophysiological basis of dystonias. Nat Rev Neurosci 9: 222–234.
44. Ferreira TL, Moreira KM, Ikeda DC, Bueno OF, Oliveira MG (2003) Effects of dorsal striatum lesions in tone fear conditioning and contextual fear conditioning. Brain Res 987: 17–24.
45. Jongen-Relo AL, Kaufmann S, Feldon J (2003) A differential involvement of the shell and core subterritories of the nucleus accumbens of rats in memory processes. Behav Neurosci 117: 150–168.
46. Frank MJ, Seeberger LC, O'Reilly RC (2004) By carrot or by stick: cognitive reinforcement learning in parkinsonism. Science 306: 1940–1943.
47. Schultz W (2002) Getting formal with dopamine and reward. Neuron 36: 241–263.
48. Seymour B, O'Doherty JP, Dayan P, Koltzenburg M, Jones AK, et al. (2004) Temporal difference models describe higher-order learning in humans. Nature 429: 664–667.
49. Yehuda R, LeDoux J (2007) Response variation following trauma: a translational neuroscience approach to understand PTSD. Neuron 56: 19–32.
50. Brunet A, Orr SP, Tremblay J, Robertson K, Nader K, et al. (2008) Effect of post-retrieval propranolol on psychophysiologic responding during subsequent script-driven traumatic imagery in post-traumatic stress disorder. J Psychiatr Res 42: 503–506.
51. Koresawa Y, Miyagawa S, Ikawa M, Matsunami K, Yamada M, et al. (2000) Synthesis of a new Cre recombinase gene based on optimal codon usage for mammalian systems. J Biochem 127: 367–372.
52. Mizushima S, Nagata S (1990) pEF-BOS, a powerful mammalian expression vector. Nucleic Acids Res 18: 5322.
53. Kim JJ, DeCola JP, Landeira-Fernandez J, Fanselow MS (1991) N-methyl-D-aspartate receptor antagonist APV blocks acquisition but not expression of fear conditioning. Behav Neurosci 105: 126–133.
54. Mangiarini L, Sathasivam K, Seller M, Cozens B, Harper A, et al. (1996) Exon 1 of the HD gene with an expanded CAG repeat is sufficient to cause a progressive neurological phenotype in transgenic mice. Cell 87: 493–506.

OPEN ACCESS Freely available online PLoS one

Ablation of NMDA Receptors Enhances the Excitability of Hippocampal CA3 Neurons

Fumiaki Fukushima[1], Kazuhito Nakao[1], Toru Shinoe[2¤a], Masahiro Fukaya[3], Shin-ichi Muramatsu[4], Kenji Sakimura[5], Hirotaka Kataoka[1], Hisashi Mori[1¤b], Masahiko Watanabe[3], Toshiya Manabe[2,6], Masayoshi Mishina[1]*

1 Department of Molecular Neurobiology and Pharmacology, Graduate School of Medicine, University of Tokyo, Tokyo, Japan, **2** Division of Neuronal Network, Institute of Medical Science, University of Tokyo, Tokyo, Japan, **3** Department of Anatomy, Hokkaido University School of Medicine, Sapporo, Japan, **4** Division of Neurology, Department of Medicine, Jichi Medical University, Tochigi, Japan, **5** Department of Cellular Neurobiology, Brain Research Institute, Niigata University, Niigata, Japan, **6** CREST, JST, Kawaguchi, Japan

Abstract

Synchronized discharges in the hippocampal CA3 recurrent network are supposed to underlie network oscillations, memory formation and seizure generation. In the hippocampal CA3 network, NMDA receptors are abundant at the recurrent synapses but scarce at the mossy fiber synapses. We generated mutant mice in which NMDA receptors were abolished in hippocampal CA3 pyramidal neurons by postnatal day 14. The histological and cytological organizations of the hippocampal CA3 region were indistinguishable between control and mutant mice. We found that mutant mice lacking NMDA receptors selectively in CA3 pyramidal neurons became more susceptible to kainate-induced seizures. Consistently, mutant mice showed characteristic large EEG spikes associated with multiple unit activities (MUA), suggesting enhanced synchronous firing of CA3 neurons. The electrophysiological balance between fast excitatory and inhibitory synaptic transmission was comparable between control and mutant pyramidal neurons in the hippocampal CA3 region, while the NMDA receptor-slow AHP coupling was diminished in the mutant neurons. In the adult brain, inducible ablation of NMDA receptors in the hippocampal CA3 region by the viral expression vector for Cre recombinase also induced similar large EEG spikes. Furthermore, pharmacological blockade of CA3 NMDA receptors enhanced the susceptibility to kainate-induced seizures. These results raise an intriguing possibility that hippocampal CA3 NMDA receptors may suppress the excitability of the recurrent network as a whole *in vivo* by restricting synchronous firing of CA3 neurons.

Citation: Fukushima F, Nakao K, Shinoe T, Fukaya M, Muramatsu S-i, et al. (2009) Ablation of NMDA Receptors Enhances the Excitability of Hippocampal CA3 Neurons. PLoS ONE 4(1): e3993. doi:10.1371/journal.pone.0003993

Editor: Frederic Andre Meunier, The University of Queensland, Australia

Received September 4, 2008; **Accepted** December 3, 2008; **Published** January 14, 2009

Funding: This work was supported in part by Grant-in-Aid for Scientific Research on Priority Areas (Molecular Brain Science) and Global COE Program (Integrative Life Science Based on the Study of Biosignaling Mechanisms) from the Ministry of Education, Culture, Sports, Science and Technology of Japan. F.F. was supported by Japan Society for the Promotion of Science, and S.T. by the 21st Century COE Program, the Ministry of Education, Culture, Sports, Science and Technology of Japan. The funders had no role in study design, data collection and analysis, decision to publish, or preparation of the manuscript.

Competing Interests: The authors have declared that no competing interests exist.

* E-mail: mishina@m.u-tokyo.ac.jp

¤a Current address: Division of Molecular and Developmental Biology, Institute of Medical Science, University of Tokyo, Tokyo, Japan,
¤b Current address: Department of Molecular Neuroscience and Pharmaceutical Sciences, Graduate School of Medicine, University of Toyama, Toyama, Japan

Introduction

Hippocampal CA3 pyramidal neurons form abundant recurrent connections with other CA3 neurons [1,2]. The activity of single pyramidal neurons spreads to other CA3 neurons and this facilitates the rapid synchronization of action-potential firing in CA3 neurons [3]. Synchronized discharges of hippocampal CA3 neurons are supposed to underlie network oscillations [4], memory consolidation [5] and seizure generation [6]. Physiological sharp wave (SPW) activity that occurs during slow-wave sleep and behavioral immobility is dependent on synchronous discharges by population of CA3 pyramidal neurons [7,8]. Synchronized CA3 activity may also contribute to the pathological EEG pattern, known as an interictal spike, which indicates a propensity for temporal lobe seizures [6].

NMDA receptors play key roles in synaptic plasticity and memory [9]. In the CA3 network, NMDA receptors are abundant at the commissural/associational synapses but scarce at the mossy fiber synapses [10]. Thus, the CA3 recurrent network is under the control of NMDA receptors. NMDA receptors in the hippocampal CA3 region are implied in rapid acquisition and recall of associative memory as well as paired associate learning [11–13]. On the other hand, studies with hippocampal slices showed that the synchronous network activity induces NMDA receptor-dependent LTP of CA3 recurrent synapses [14] and that stimuli that induced NMDA receptor-dependent LTP in the CA3 region generated sharp wave-like synchronous network activity [15]. These *in vitro* observations raised the hypothesis that the NMDA receptor-mediated LTP contributes to the generation of synchronous network activity. Here, we generated hippocampal CA3 pyramidal neuron-specific NMDA receptor mutant mice on the pure C57BL/6N genetic background. The ablation of hippocampal CA3 NMDA receptors resulted in the enhancement of the susceptibility to kainate-induced seizure and the emergence of characteristic large EEG spikes. We also showed that the virus-mediated ablation of hippocampal CA3 NMDA receptors in the

adult mice generated characteristic large EEG spikes and that pharmacological blockade of CA3 NMDA receptors enhanced the susceptibility to kainate-induced seizures. These results raise an intriguing possibility that NMDA receptors may control negatively the excitability of the hippocampal CA3 recurrent network as a whole *in vivo*.

Methods

Generation of mice

Genomic DNA carrying the exon 11 to 22 of the *GluRζ1* gene was isolated by screening a bacterial artificial chromosome (BAC) library prepared from the C57BL/6 strain (Incyte Genomics) with the 2.2 kb-*Eco*RI fragment from pBKSAζ1 [16]. The 13.3-kb *Eco*RI-*Xba*I fragment of the BAC clone was used for construction of the targeting vector. The *loxP* site was inserted into the *Bam*HI site between exon 18 and 19, and the 1.8-kb DNA fragment carrying the *loxP* sequence and *Pgk-1* promoter-driven neomycin phosphotransferase gene (*neo*) flanked by two Flp recognition target (*frt*) sites into the *Spe*I site between exon 20 and 21. Endogenous *Eco*RI site at the 5′ end of 13.3-kb *Eco*RI-*Xba*I genomic fragment was replaced with *Not*I site and an exogenous *Eco*RI site was inserted between the second *loxP* site and *neo* gene. The targeting vector pζ1TV was composed of the 14.8-kb *Not*I-*Xba*I fragment, MC1 promoter-driven diphteria toxin gene derived from pMC1DTpA and pBluescript II SK(+) [17]. The targeting vector was linearized by *Not*I and electroporated into ES cells derived from the C57BL/6N strain [18,19]. Recombinant clones were identified by Southern blot analysis of *Eco*RI-digested genomic DNA using 284-bp fragment amplified with primers 5′-ATAGA-GAAAGACATGGGGC-3′ and 5′-TGCTACTGTGCAG-GAAGTG-3′ from pζ1TV, the 0.6 kb *Pst*I fragment from pLFNeo [20], and the 1.1-kb *Xho*I–*Eco*RI fragment from the BAC clone as 5′ inner, neo, and 3′ outer probes, respectively. The $GluR\zeta1^{flox}$ allele was also identified by PCR using primers 5′-GCAGT-GAGGCTCACACAGGCCTGAAGACTA-3′ and 5′-AGT-GAACTCGGATCCTGACCATTGGCCACT-3′. Chimeric mice production and elimination of the *neo* gene from the genome through Flp/frt-mediated excision were carried out essentially as described [18–20].

GluRγ1-Cre mice were obtained by inserting the *cre* gene in the translational initiation site of the *GluRγ1* gene in frame using ES cells derived from the C57BL/6N strain [19]. The 1.8-kb DNA fragment, which carried the polyadenylation signal sequence and *pgk-1* promoter-driven *neo* gene flanked by two *frt* sites [20], was inserted into the downstream of the *cre* gene. $GluR\zeta1^{+/flox}$ mice were crossed with GluRγ1-Cre mice to yield $GluR\gamma1^{+/cre}$; $GluR\zeta1^{flox/flox}$ mice. The $GluR\gamma1^{+/cre}$ allele was identified by PCR using primers 5′-AACTGCAGTCTTGCATGCTCTCTG-GAGCC-3′, 5′-GGAGCGGAGACACGGGGCAT-3′ and 5′-TTGCCCCTGTTTCACTATCC-3′. Cre recombinase-mediated NMDA receptor ablation is hippocampal CA3 pyramidal neuron-specific in $GluR\gamma1^{+/cre}$; $GluR\zeta1^{flox/flox}$ mice (Fig. 1). It is unknown why the *GluRγ1* promoter-driven Cre expression does not exactly follow the expression pattern of GluRγ1 [21]. The insertion of the *pgk-1* promoter-driven *neo* gene and the polyadenylation signal sequence together may affect the Cre expression pattern since the elimination of the *neo* gene through Flp-mediated recombination altered the expression pattern.

All animal procedures were approved by the Animal Care and the Use Committee of Graduate School of Medicine, the University of Tokyo (Approval # 1721T062). Mice were fed *ad libitum* with standard laboratory chow and water in standard animal cages under a 12 h light/dark cycle.

AAV-Cre vector

We employed AAV to deliver Cre recombinase since AAV is safe, non-pathogenic, non-inflammatory and extremely stable stable [22,23]. AAV-Cre or AAV-EGFP vector contains an expression cassette consisting of a human cytomegalovirus immediate-early promoter (CMV promoter), followed by the human growth hormone first intron, cDNA of Cre recombinase with a nuclear localization signal or the enhanced green fluorescence protein (EGFP), and simian virus 40 polyadenylation signal sequence (SV40 polyA), between the inverted terminal repeats (ITR) of the AAV-2 genome. The two helper plasmids, pAAV-RC and pHelper (Agilent Technologies, Santa Clara, California), harbor the AAV *rep* and *cap* genes, and the *E2A*, *E4*, and *VA RNA* genes of the adenovirus genome, respectively. HEK293 cells were cotransfected by the calcium phosphate coprecipitation method with the vector plasmid, pAAV-RC, and pHelper. AAV vectors were then harvested and purified by two sequential continuous iodoxale ultracentrifugations. The vector titer was determined by quantitative DNA dot-blot hybridization or quantitative PCR of DNase-I-treated vector stocks. Before administration, AAV vectors were diluted in phosphate-buffered saline to $5–8\times10^{10}$ genome copies/μl. A glass micropipette was inserted into the hippocampal CA3 region of ketamine-anesthetized mice (AP, L, V = −1.2, ±1.2, +2.0; −1.7, ±2.0, +2.1; −2.2, ±2.5, +2.4; −2.7, ±3.2, +3.5; −3.2, ±2.5, +4.0). Two minutes after the insertion, 1.0 μl of a virus solution or vehicle was injected at a constant flow rate of 16.6 nl/min, and the glass micropipette was left in this configuration for an additional 2 min, to prevent reflux of the injected material along the injection track, before being slowly retracted. AAV spread 0.5–0.7 mm both rostrodorsally and laterally. For every injected animal, the limit of the infected region was verified by immunohistochemistry for Cre recombinase or GluRζ1.

Immunological analysis

Immunohistochemistry was done as described [24] using antibodies against VGluT2 (guinea pig) [25], Calbindin (rabbit) [26], PSD-95 (rabbit) [27], GluRα1 (rabbit) [28], GAD (guinea pig) [29], and Cre recombinase (1:1000; rabbit; Novagen). Immunobloting analyses in whole-brain homogenate were carried out using antibodies for GluRζ1 (rabbit) [30], and neuron-specific enolase (1:4000; Chemicon) and chemiluminescense (Amersham Biosciences).

Golgi staining

Coronal brain sections (2 mm) were immersed for 4 days in a solution composed of 5% glutaraldehyde (Wako) and 2% $K_2Cr_2O_7$ (Sigma) and then transferred to a 0.75% solution of $AgNO_3$ (Sigma) for further 4 days. The treated brain was sectioned (100 μm), dehydrated and mounted on glass slides.

Morphology of AAV-EGFP infected CA3 neurons

AAV-EGFP vector was delivered into the hippocampal CA3 region of ketamine-anesthetized control and mutant mice of 8 weeks old. Fourteen days later, fixed coronal brain sections (150 μm) were prepared. Neurons were examined with a Leica SP-5 confocal laser scanning microscope. Optical sections were collected at intervals of 0.15 μm and averaged 16 times using a 100×objective (N.A. 1.4). The distance between axonal varicosities was measured from 50 μm-portions of CA3 axons within the CA3 stratum radiatum [31]. For spine analysis, only spines on clearly visible tertiary apical and basal branches were imaged. During the quantitation of the spine density, putative spines in the

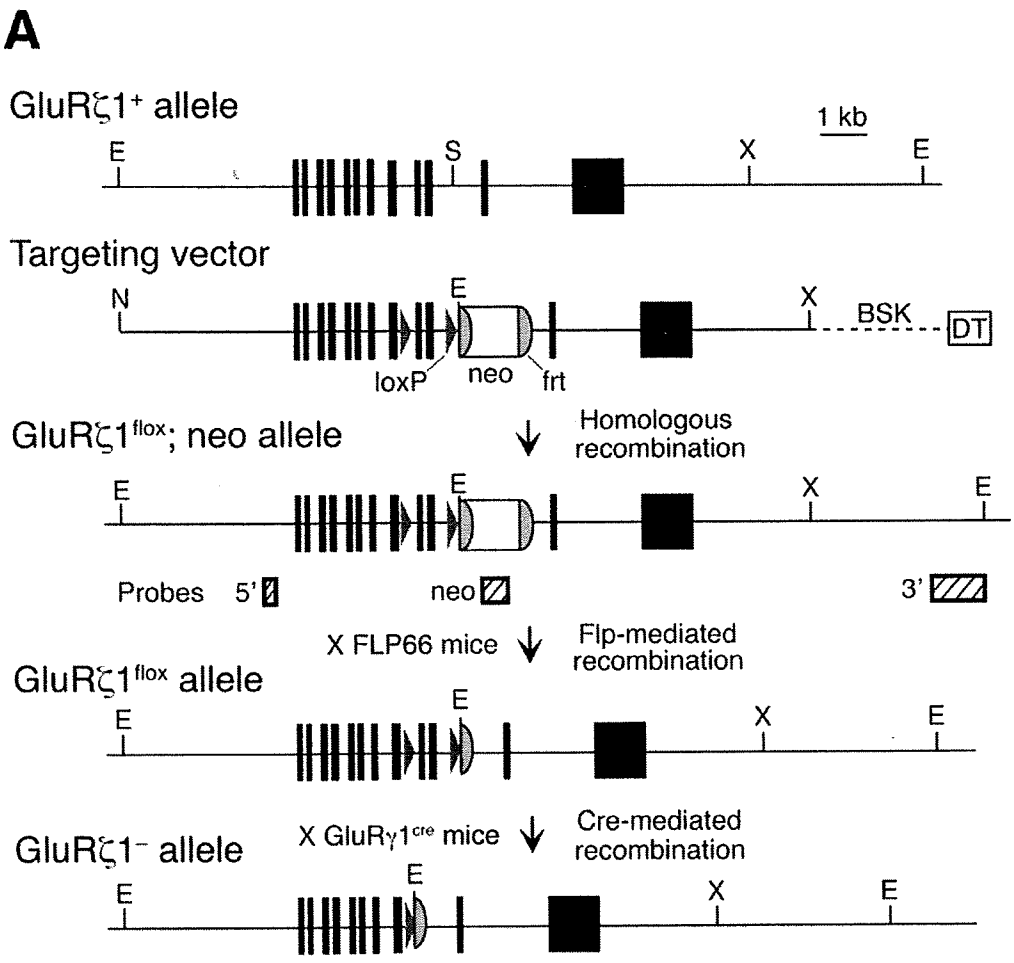
A
GluRζ1+ allele
1 kb
E
S
X
E
Targeting vector
N
E
X
BSK
DT
loxP
neo
frt
GluRζ1flox; neo allele
Homologous recombination
E
E
X
E
Probes 5'
neo
3'
X FLP66 mice
Flp-mediated recombination
GluRζ1flox allele
E
X
E
GluRζ1- allele
X GluRγ1cre mice
Cre-mediated recombination
E
X
E

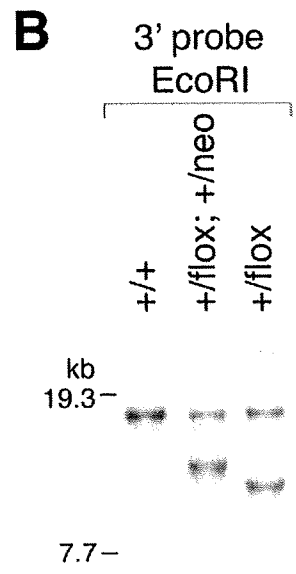
B
3' probe
EcoRI
+/+
+/flox; +/neo
+/flox
kb
19.3
7.7

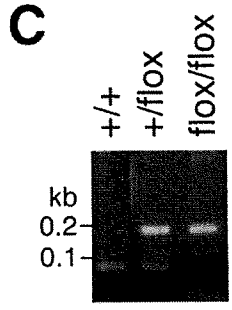
C
+/+
+/flox
flox/flox
kb
0.2
0.1

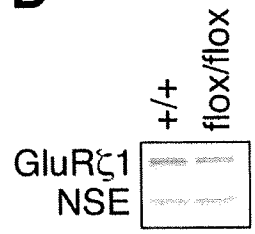
D
+/+
flox/flox
GluRζ1
NSE

Figure 1. Generation of *GluRζ1*^{flox} mice by homologous recombination in C57BL/6 strain derived ES cells. A, Schema of the exons 11–22 region of the *GluRζ1* gene (*GluRζ1*$^{+}$), targeting vector, floxed and *neo*-inserted allele (*GluRζ1*^{flox}; *neo*), and floxed allele (*GluRζ1*^{flox}). Exons 19 and 20 encode the putative transmembrane segment M4 of GluRζ1. The *GluRζ1*^{flox}; *neo* allele contains two *loxP* sequences flanking exons 19 and 20 of the *GluRζ1* gene and the *neo* gene flanked by two *frt* sequences. The *neo* gene was removed *in vivo* by crossing *GluRζ1*$^{+/flox}$; +/*neo* mice with FLP66 mice carrying the Flp recombinase gene under the control of the *EF1α* promoter. *GluRζ1*$^{+/flox}$ mice were crossed with GluRγ1-Cre mice to disrupt the GluRζ1 gene selectively in the hippocampal CA3 region. Abbreviations: BSK, plasmid pBluescript; DT, diphtheria toxin gene; neo, neomycin phosphotransferase gene; E, *Eco*RI; N, *Not*I; S, *Spe*I; X, *Xba*I. Hatched boxes indicate the location of probes for Southern blot analysis. **B**, Southern blot analysis of genomic DNA from *GluRζ1*$^{+/+}$, *GluRζ1*$^{+/flox}$; +/*neo*, and *GluRζ1*$^{+/flox}$ mice. *Eco*RI-digested DNA was hybridized with 3′ probe. **C**, Agarose gel electrophoresis of DNA fragments amplified by PCR from *GluRζ1*$^{+/+}$, *GluRζ1*$^{+/flox}$ and *GluRζ1*$^{flox/flox}$ mice. The amplified DNA fragments derived from the *GluRζ1*$^{+}$ and *GluRζ1*^{flox} alleles were 61 bp and 169 bp, respectively. **D**, Western blot analysis of GluRζ1 and neuron-specific enolase (NSE) proteins in whole-brain homogenates from *GluRζ1*$^{+/+}$ and *GluRζ1*$^{flox/flox}$ mice.
doi:10.1371/journal.pone.0003993.g001

three-dimensional reconstructed image were compared with both the unprocessed, individual optical sections and with a 'movie', in which segments of the three-dimensional reconstruction were rotated around the dendritic axis (IMARIS, Bitplane). For dendritic analysis, neurons were imaged on a Leica SP-5 with a 40×objective (N.A. 0.8). Optical sections were collected at intervals of 2 μm and averaged 8 times. The topographical order of the dendritic tree was made using the semi-automated program FilamentTracer (Bitplane). Analysis of dendritic topology included dendritic branches up to the third order. Analysis of dendritic spines was performed in rather linear, apical secondary and tertiary dendrites.

In situ hybridization

Isotopic detection of mRNAs was performed as described [32]. All samples were subjected to hybridization analysis at the same time and sections were exposed to a single x-ray film for measurement of relative optical density with IP Lab software. The relative expression levels of the mRNAs in the hippocampal CA3 region were calculated using the ratio of the density in the CA3 region to that of the CA1 region, except that the *GluRγ1* mRNA density in the CA3 region was directly compared between control and mutant mice. Double *in situ* hybridization was performed with mixture of [^{33}P]dATP-labeled oligonucleotide probe for GluRζ1 (complementary to residues 2583–2627, GenBank accession No. D10028) and digoxigenin (DIG)-labeled cRNA probe for GAD67 (complementary to residues 802–1617, No. A28072) as described [33]. Hybridization signals were visualized with nuclear track emulsion (NTB-2, Kodak) and fluorescent substrate (HNPP Fluorescent Detection Set, Boehringer-Mannheim), respectively. Sections were counterstained with NeuroTrace 500/525 green (Molecular Probes).

Kainate-induced seizure

Kainate was intraperitoneally administered to mice, and they were monitored for 1 h to determine whether they exhibited seizures with generalized tonic-clonic activity accompanying the loss of postural tone. Mice were then fixed under deep pentobarbital anesthesia for immunohistochemical analysis with the c-Fos antibody (Oncogene) 2 h after kainate administration.

Electrophysiology

Transverse hippocampal slices (400 μm thick) were superfused with an artificial cerebrospinal fluid (aCSF) containing (in mM): 119 NaCl, 2.5 KCl, 2.5 $CaCl_2$, 1.3 $MgSO_4$, 1 NaH_2PO_4, 26.2 $NaHCO_3$, and 11 glucose, which was equilibrated with 95% O_2/5% CO_2. Synaptic responses were evoked via a bipolar stimulating electrode placed in the CA3 stratum radiatum and whole-cell recordings were made from CA3 pyramidal cells using the blind-patch technique. The stimulus strength was set at the beginning of each experiment so that the average amplitude of synaptic responses in the absence of any antagonists is around 200 pA at a holding potential of −80 mV. The AMPA receptor-mediated excitatory postsynaptic current (AMPA-EPSC) was isolated by subtracting the synaptic response in the presence of 10 μM 6-cyano-7-nitroquinoxaline-2,3-dione (CNQX) from that in its absence. The NMDA receptor-mediated excitatory postsynaptic current (NMDA-EPSC) was recorded at +50 mV in the presence of 10 μM CNQX and 0.1 mM picrotoxin. The $GABA_A$ receptor-mediated inhibitory postsynaptic current ($GABA_A$-IPSC) was recorded at 0 mV in the presence of 10 μM CNQX and 25 μM D-2-amino-5-phosphonovaleric acid (D-APV). The stimulus strength was constant throughout each experiment. The slow hyperpolarizing currents induced by high-frequency stimulation (50 Hz, 40 pulses) were recorded at −20 mV in the presence of 0.1 mM picrotoxin as described previously [34]. Patch electrodes were filled with an internal solution containing (in mM): 140 potassium methansulfonate, 8 NaCl, 10 HEPES, 2 MgATP, and 0.3 Na_3-GTP (pH 7.2 adjusted with KOH, osmolarity 290 to 300 mOsm). For pharmacological experiments, 10 mM BAPTA was added in the pipette solution or potassium methansulfonate in the pipette solution was replaced by cesium methansulfonate. Voltage-clamped responses were recorded with an Axopatch 1D amplifier (Axon Instruments, Union City, CA, USA) and the signal was filtered at 1 kHz, digitized at 2.5 kHz, and stored on a personal computer.

Field potential recording *in vivo*

Urethane-anesthetized mice (1 g/kg body weight, i.p.) were fixed in a stereotaxic head holder (Narishige). For the recording of local field potentials, a tungsten electrode (2–5 MΩ, Frederick Haer) or a silicon probe (16 recoding sites with 50 μm separation, NeuroNexus Technologies) was inserted into the hippocampal CA3 region (AP = −2.0 mm from bregma, L = ±2.3 mm from midline, and V = +2.0 mm ventral to dura), the hippocampal CA1 region (AP = −2.0, L = ±1.0, V = +1.2) or the dentate gyrus (AP = −2.0, L = ±1.0, V = +2.0). Signals were amplified (MEG-1200, Nihon Kohden), band-pass filtered (0.08–1,000 Hz), digitized at 1 kHz through an AD converter (National Instruments), and stored in a computer. Analyses of data were performed offline using LabVIEW (National Instruments) and IGOR (Wave matics) software. Recordings using a glass electrode (10–15 MΩ, GD-2, Narishige) were carried out as described [35]. Raw traces (0.08–3,000 Hz) were band-pass filtered for the detection of MUA of neurons (0.15–3 kHz). EEG spikes with power of twice the s.d. from the baseline mean and the duration of about 30 ms were extracted. The unit activity was defined as a power of more than five times the s.d. from the baseline mean and the duration of less than 4 ms [7]. The locations of the electrode were verified histologically. CSD analyses were carried out as described [8].

Pharmacological experiments. Mice were anesthetized with ketamine (80 mg/kg, i.p.; Sankyo Co., Tokyo, Japan) and xylazine (20 mg/kg i.p.; Bayer, Tokyo, Japan), and fixed to a

stereotaxic apparatus (David Kopf, Tujunga, CA, USA). Two single guide cannulae (Plastics One, Roanoke, VA, USA) were implanted into the CA3 region of the hippocampus bilaterally (stereotaxic coordinates: AP = −2.2 mm from bregma, ML = ±2.5 mm from midline, DV = +1.4 mm from bregma), according to an atlas of the mouse brain [36]. The tip of the internal cannula for microinjection was inserted 1 mm below the tip of the guide cannulae (DV = +2.4 mm from bregma). The cannulae were fixed to the skull with dental cement. The animals were allowed to recover for at least 5 days. D,L-APV (Sigma-Aldrich, MO, USA) was dissolved in aCSF at a concentration of 30 mM. The aCSF was consisted of NaCl (150 mM), KCl (3 mM), $CaCl_2$ (1.4 mM), $MgCl_2$ (0.8 mM), Na_2HPO_4 (0.8 mM), and NaH_2PO_4 (0.2 mM). During drug infusions, the mice were restrained lightly in the disposable vinyl jacket (Braintree Scientific, Inc, MA, USA) and 0.5 µl of the drug or aCSF was infused at a rate of 0.2 µl/min using a microinjection pump (CMA/100, CMA/Microdialysis, Solna, Sweden). The infusion cannulae (bilateral) were left in place for a further 1 min to diffuse the drug from the needle tip, and the animal was then returned to its home cage. Kainate was delivered i.p. 20–30 min after APV injection.

Statistical analysis

All behavioral experiments were performed in a blind fashion. Data were expressed as mean±SEM. Statistical analysis was performed using Fisher's exact probability test, Kolmogorov-Smirnov test, log-rank test and Student *t*-test as appropriate. Statistical significance was set at $p<0.05$.

Results

Selective ablation of NMDA receptors in hippocampal CA3 pyramidal neurons

We disrupted the NMDA receptor *GluRζ1/NR1* gene specifically in the hippocampal CA3 pyramidal cells by Cre-*loxP* recombination on the C57BL/6N genetic background. By crossing a target mouse line carrying two *loxP* sequences flanking exon 19 and 20 of the *GluRζ1* gene (*GluRζ1*$^{+/flox}$ mice) with a hippocampal CA3 region-dominant Cre mouse line carrying the Cre recombinase gene inserted into the *GluRγ1/KA-1* gene (GluRγ1-Cre mice), we obtained *GluRγ1*$^{+/cre}$; *GluRζ1*$^{flox/flox}$ mice and *GluRζ1*$^{flox/flox}$ mice (Fig. 1), and used them in subsequent experiments as mutant and control mice, respectively.

In situ hybridization signals for the *GluRζ1* mRNA were indistinguishable between mutant and control mice at postnatal day 1 (P1) (Fig. 2A). At P7, *GluRζ1* signals were diminished specifically in the hippocampal CA3 region of mutant mice (Fig. 2B). At P21 to P23, the hybridization signals were hardly detectable in the CA3 region of mutant mice and slightly decreased in the brainstem (Fig. 2C). Residual hybridization signals for the *GluRζ1* mRNA were co-localized with those of the *GAD67* mRNA, suggesting that expression of the *GluRζ1* mRNA was intact in CA3 interneurons (Fig. 2G, $n = 17$ out of 17 GAD67-positive cells). Immunohistochemical analyses showed that immunoreactivity for GluRζ1 protein was present in the CA3 region at P7, though the amount appeared to be decreased (Fig. 2D). However, the expression of GluRζ1 protein was diminished to a negligible level at P14 and P21 (Fig. 2E and F).

We examined NMDA-EPSCs by whole-cell patch-clamp recordings from the pyramidal cell in the CA3 region of the hippocampus at P21 to P23. NMDA-EPSCs were evoked by stimulating associational/commissural fibers that mainly terminate in the stratum radiatum since NMDA receptors are more

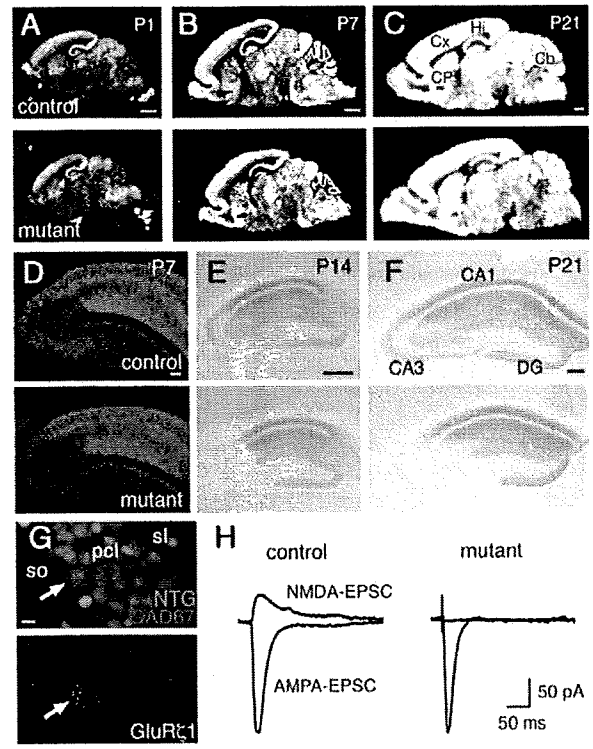

Figure 2. Generation of CA3 pyramidal neuron-selective NMDA receptor knockout mice. A–C, X-ray film autoradiography for *GluRζ1* mRNAs. Arrowheads indicate the CA3 region. **D–F**, Immunohistochemistry for GluRζ1 proteins. **G**, Double *in situ* hybridization for *GluRζ1* (white) and *GAD67* mRNA (red), counterstained with neurotrace green (green), in the mutant CA3 region. Arrow indicates a neuron expressing both *GluRζ1* and *GAD67* mRNAs. Scale bars: **A–C**, 1 mm; **D–F**, 200 µm; **G**, 10 µm. Abbreviations: Cb, cerebellum; CP, caudate-putamen; Cx, cortex; DG, dentate gyrus; Hi, hippocampus; pcl, pyramidal cell layer; sl, stratum lucidum; so, stratum oriens. **H**, Representative traces of AMPA- and NMDA-EPSCs at CA3 commissural/associational synapses.
doi:10.1371/journal.pone.0003993.g002

abundantly expressed in the stratum radiatum than in the stratum lucidum (Fig. 2H). In mutant mice, NMDA-EPSCs were not detectable, while AMPA-EPSCs were normally evoked. The ratios of the amplitudes of NMDA-EPSCs to those of AMPA-EPSCs were 50.9±16.1% (mean±s.e.m.) in control mice and 0.2±0.2% in mutant mice ($n = 4$ each; *t*-test, $P = 0.03$). Thus, NMDA receptors were abolished in hippocampal CA3 pyramidal neurons of mutant mice by P21. We used mutant and control mice at P21 to P23 in the following experiments unless otherwise specified.

Enhanced susceptibility of mutant mice to kainate-induced seizure

To monitor the excitability of CA3 recurrent circuits *in vivo*, we tested the kainate sensitivity of mutant mice since the administration of kainate to rodents stimulates initially the CA3 region and then generates seizures [37]. Intraperitoneal administration of kainate at 8 mg/kg induced tonic-clonic seizures with loss of the postural tone in mutant mice within 1 h, but not in control mice (Fig. 3A, $P<0.001$, Fisher's exact probability test). Mice of both genotypes showed seizures at a higher dosage of kainate (12 mg/kg), but the latency to the onset of seizures was significantly shorter in mutant mice (Fig. 3B, $P = 0.03$, log-rank test). Neither mutant

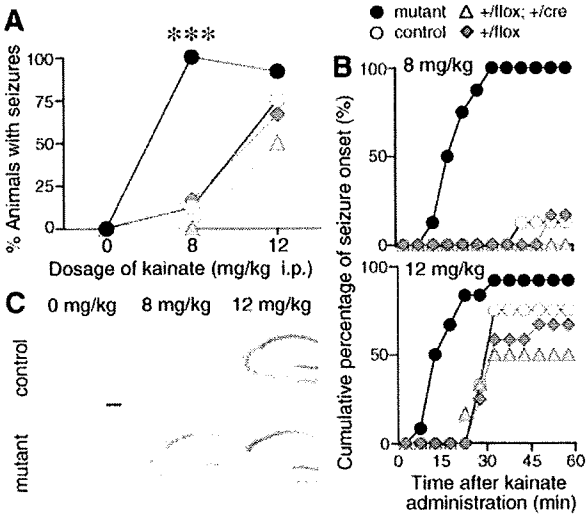

Figure 3. Increased susceptibility to kainate-induced tonic-clonic seizures in the mutant mice. A, The graph represents the percentage of mice with the generalized tonic-clonic seizures 1 h after drug administration. ***, $P<0.001$, Fisher's exact probability test. **B**, Cumulative curves for the onset of seizure. Saline, $n=4$–6; 8 mg/kg, $n=7$–8; 12 mg/kg, $n=12$. **C**, c-Fos immunohistochemistry in the hippocampus. Scale bar, 200 μm.
doi:10.1371/journal.pone.0003993.g003

nor control mice showed seizures after saline-administration. These results suggest that kainate-induced seizure susceptibility was enhanced in mutant mice. Susceptibility to the seizure was comparable between control *GluRζ1*$^{flox/flox}$ mice and *GluRγ1*$^{+/cre}$; *GluRζ1*$^{+/flox}$ mice, indicating that the insertion of the *Cre* gene in one allele of *GluRγ1* locus did not influence the susceptibility.

To monitor the neuronal activity *in vivo*, we employed c-Fos immunohistochemistry. There was little c-Fos immunoreactivity in the hippocampus of both control and mutant mice administrated with saline ($n=3$, Fig. 3C). Administration of kainate at 8 mg/kg induced strong c-Fos-immunoreactivity in the hippocampus of mutant mice ($n=3$). In contrast, no significant immunoreactivity was detectable in the hippocampus of kainate-administrated control mice ($n=3$). Kainate at 12 mg/kg induced strong c-Fos immunoreactivity in both control and mutant mice with seizures, while the number of Fos-immunopositive cells in the hippocampus was significantly smaller in mutant mice than in control mice ($n=20$ sections from 5 mice). The cellular imaging of neural activity with c-Fos immunohistochemistry confirmed the enhanced seizure susceptibility of mutant mice.

Histological features of the hippocampal CA3 region

Unexpectedly, we found that mutant mice lacking NMDA receptors selectively in CA3 pyramidal neurons became more susceptible to kainate-induced seizures. One obvious possibility is that the ablation of NMDA receptors may disturb the neural wiring of the hippocampal CA3 region, leading to abnormal excitability of the network. We thus examined the histological features of the hippocampal CA3 region in detail. The laminar organization and cellular distribution of the hippocampal CA3 region examined by Nissl staining was indistinguishable between control and mutant mice (Fig. 4A). Immunostaining for vesicular glutamate transporter 2 (VGluT2) and calbindin showed that the afferent terminals from the entorhinal cortex and the dentate gyrus were localized in the stratum lacunosum-moleculare and the stratum lucidum in both control and mutant mice, respectively (Fig. 4B and C).

Golgi staining revealed no appreciable differences in dendritic arborization of CA3 pyramidal cells between control and mutant mice (Fig. 4G). There were no significant differences in the numbers of branch points (control, 16.6±1.1, $n=8$; mutant, 17.0±1.1, $n=9$; $P=0.80$; *t*-test) and the primary (control, 4.4±0.5; mutant, 3.8±0.6; $P=0.45$), secondary (control, 7.8±0.7; mutant, 7.0±0.7; $P=0.49$) and tertiary dendrites (control, 9.4±1.4; mutant, 9.9±1.0; $P=0.76$) between two genotypes (Fig. 4I and J). Mean spine density on basal dendrites of CA3 pyramidal cells was also comparable ($n=28$ dendrites from 3–4 mice, $P=0.15$) (Fig. 4H and K). Consistent with Golgi staining, fine structures of CA3 neurons visualized by EGFP expression revealed no detectable alteration in terms of dendritic arborization and the distribution of presynaptic axonal boutons and postsynaptic spines (Fig. 5).

Immunoreactivities for postsynaptic proteins, PSD-95 and GluRα1/GluR1, were comparable in the hippocampal CA3 region between the two genotypes (Fig. 4D and E). Distribution of interneurons in the hippocampal CA3 and hilar areas was also indistinguishable as judged by immunostaining for GAD proteins (Fig. 4F), parvalbumin, somatostatin and calretinin. Thus, the histological and cytological organizations of the hippocampal CA3 region were indistinguishable between control and mutant mice.

Characteristic EEG spikes associated with multiple unit activities in the hippocampal CA3 region of mutant mice

Since seizure is produced by synchronous firing of a population of neurons in the brain [38], it is possible that NMDA receptor ablation in the CA3 region may modify hippocampal network oscillations *in vivo*. By recording local field potentials *in vivo* from the hippocampal CA3 region of urethane-anaesthetized mutant mice at the age of postnatal 8 weeks, we found characteristic spikes with large amplitudes (1.5–4.0 mV) (Fig. 6A). These EEG spikes were consistently observed in all 6 mutant mice, but never detected in 7 control mice. The mean firing rate of the spikes ($n=136$ from 6 mice) was 0.23±0.02 Hz and the distribution of interspike intervals showed a peak at 4.75 s (Fig. 6B).

To investigate the origin of characteristic EEG spikes, we recorded field potentials in various hippocampal regions of mutant mice using a silicon probe with 16 recording sites. Simultaneous recording of a single EEG spike event from the hippocampal CA3 region and surrounding neocortex showed that the amplitude of EEG spikes was largest in the CA3 pyramidal cell layer. EEG spikes reversed their polarity in the CA3 stratum oriens (Fig. 6C). Current source density (CSD) analysis of EEG spikes revealed a current sink in the CA3 pyramidal cell layer, with a source nearby ($n=8$ from 4 mice). Recording from the cortex and hippocampal CA1 region, spikes reversed their polarity in the CA1 stratum oriens. CSD analyses revealed a large sink in the CA1 pyramidal cell layer ($n=8$ from 4 mice). On the other hand, EEG spikes recorded from the dentate gyrus showed neither polarity reversal nor sinks in CSD maps ($n=8$ from 4 mice). These results suggest that characteristic spikes are generated in the pyramidal cell layers of the CA3 and CA1 regions, but not in the dentate gyrus.

Further analysis revealed that the frequency of MUA in the CA3 pyramidal cell layer was enormously high during spike events (Fig. 6D, center). The strong correlation between MUA and EEG spikes was observed in all 4 mutant mice. After EEG spikes, MUA in the CA3 pyramidal cell layer became silent (Fig. 6D, center). MUA in the CA1 pyramidal cell layer were also associated with EEG spikes (Fig. 6D, right) and the association was reproducibly observed in all 4 mutant mice. On the other hand, there was no

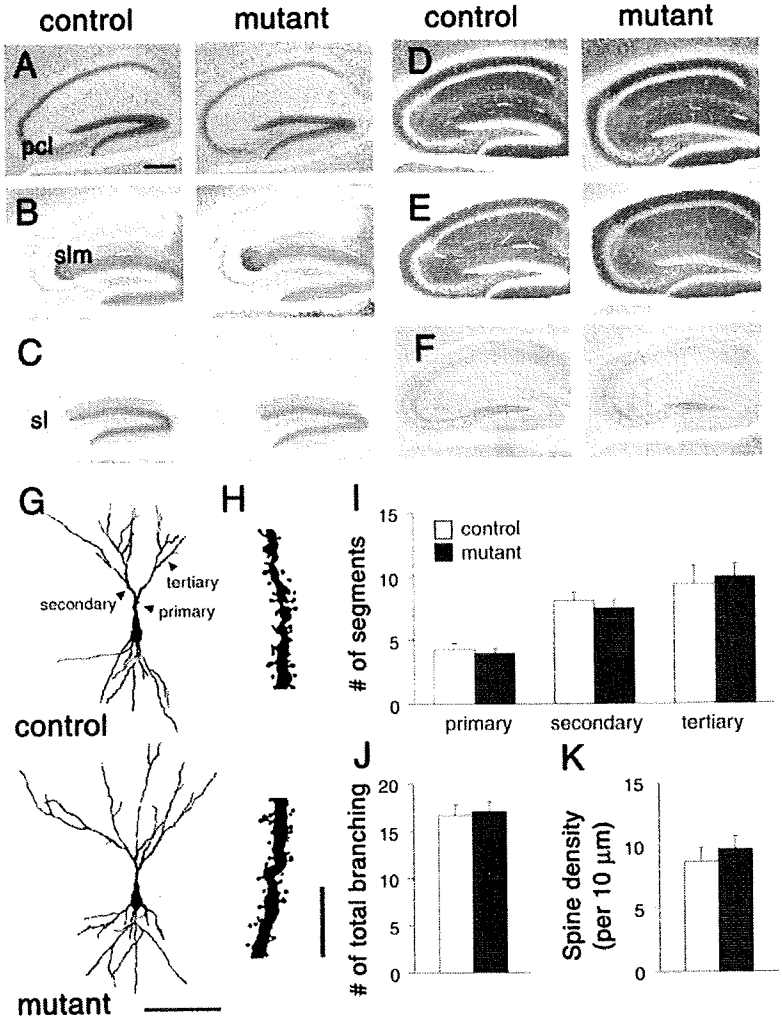

Figure 4. Normal histological organization of the hippocampal region. A, Nissl staining. **B, C**, Immunoperoxidase staining for VGluT2 (**B**) and Calbindin (**C**). **D–F**, Immunoperoxidase staining for PSD-95 (**D**), GluRα1 (**E**), and GAD (**F**). **G**, Cytoarchitecture of Golgi-stained CA3 pyramidal neurons. **H**, Higher magnification of the basal dendritic segment of CA3 pyramidal neuron in (**G**). **I–K**, Graphs represents the number of primary, secondary and tertiary dendrites (**I**), total number of dendritic branching (**J**), and spine density (**K**) of CA3 pyramidal neurons. Scale bars: **A**, 200 µm; **G**, 100 µm; **I**, 10 µm. Abbreviations: pcl, pyramidal cell layer; sl, stratum lucidum; slm, stratum lacunosum-moleculare.
doi:10.1371/journal.pone.0003993.g004

significant association in the dentate gyrus between MUA and spikes (Fig. 6D, left). The strong association of MUA with EEG spikes in the CA1 and CA3 pyramidal cell layers, but not in the dentate gyrus, together with CA3 pyramidal neuron-selective ablation of NMDA receptors, suggests that characteristic EEG spikes were originated from synchronous firing of CA3 pyramidal neurons and the activity of the CA3 network propagated to the downstream CA1 region.

Balanced excitatory and inhibitory synaptic transmission

Because either enhanced excitation or reduced inhibition can increase the excitability of hippocampal CA3 network, we examined the mRNA levels of excitatory glutamate receptor (GluR) subunits and glutamic acid decarboxylases (GADs) expressed in the hippocampal CA3 region of the mutant mice by *in situ* hybridization (Fig. 7A, Table 1). The *GluRζ1* mRNA was strongly diminished as described above. The reduction of the *GluRy1* mRNA can be ascribed to the insertion of *cre* into one allele of the *GluRy1* gene but the *cre* insertion exerted little effect on the kainate-induced seizure susceptibility as described above. There was no significant difference in the *GAD65* mRNA ($P=0.08$), while the level of *GAD67* mRNA was slightly but significantly reduced in the mutant mice ($P<0.001$). There were no significant differences in hybridization signals of other GluR mRNAs between control and mutant mice.

Basic electrophysiological properties of CA3 pyramidal cells were indistinguishable between two genotypes (resting membrane potential: control, -72.5 ± 0.8 mV, $n=32$; mutant -73.7 ± 1.0 mV, $n=26$, $P=0.37$; input resistance: control, 113.2 ± 5.3 MΩ; mutant, 117.7 ± 7.2 MΩ, $P=0.62$; membrane capacitance: control, 251.8 ± 9.4 pF; mutant, 250.2 ± 8.0 pF, $P=0.90$). We then compared $GABA_A$-IPSCs in the hippocampal CA3 region, which have been shown to suppress the excitability of the pyramidal cell through postsynaptic inhibition [39]. AMPA-EPSCs were evoked at −80 mV by stimulating afferent fibers in the CA3 stratum radiatum, which should activate both associa-